New age constraints reveal moraine stabilization thousands of years after deposition during the last deglaciation of western New York, USA

Karlee K. Prince[1], Jason P. Briner[1], Caleb K. Walcott[1], Brooke M. Chase[1], Andrew L. Kozlowski[2], Tammy M. Rittenour[3], Erica P. Yang[1,4]

[1] Department of Geology, University at Buffalo, 126 Cooke Hall, Buffalo, NY 14260, USA
[2] New York State Geological Survey, New York State Museum, 222 Madison Ave, Albany, NY 12230, USA
[3] Department of Geoscience, Utah State University, 4505 Old Main Hill, Logan, UT 84322, USA
[4] Oak Ridge Institute of Science and Education, 1299 Bethel Valley Road, Oak Ridge, TN, 37830 USA

Correspondence to: Karlee K. Prince (karleepr@buffalo.edu)

Abstract. The timing of the last deglaciation of the Laurentide Ice Sheet in western New York is poorly constrained. The lack of direct chronology in the region has led to a hypothesis that the Laurentide Ice Sheet re-advanced to near its Last Glacial Maximum terminal position in western New York at ~13 ka, which challenges long-standing datasets. To address this hypothesis, we obtained new chronology from the Kent (terminal) and Lake Escarpment (first major recessional) moraines using radiocarbon ages in sediment cores from moraine kettles supplemented with two optically stimulated luminescence ages from topset beds in an ice-contact delta. The two optically stimulated luminescence ages date the Kent (terminal) position to 19.8 ± 2.6 and 20.6 ± 2.9 ka. Within the sediment cores, there is sedimentologic evidence of an unstable landscape during basin formation; radiocarbon ages from the lowest sediments in our cores are not in stratigraphic order and date from 19,350-19,600 to 14,050-14,850 cal BP. We interpret these ages as loosely minimum-limiting constraints on ice sheet retreat. Our oldest radiocarbon age of 19,350-19,600 cal BP – from a rip-up clast – suggests ice-free conditions at that time. Above the lowest sediments there is organic-rich silt and radiocarbon ages in stratigraphic order. We interpret the lowest ages in these organic-rich sediments as minimum-limiting constraints on kettle basin formation. The lowest radiocarbon ages from organic-rich sediments from sites on both Kent and Lake Escarpment moraines range from 15,000-15,400 to 13,600-14,000 cal BP. We interpret the 5 kyr lag between the optically stimulated luminescence ages and kettle basin formation as the result of persistent buried ice in ice-cored moraines until ~15 to 14 ka. The cold conditions associated with Heinrich Stadial 1 may have enabled the survival of ice-cored moraines until after 15 ka, and in turn, climate amelioration during the Bølling Period (14.7 – 14.1 ka) may have initiated landscape stabilization. This model potentially reconciles the sedimentological and chronological evidence underpinning the re-advance hypothesis, which instead could be the result of moraine instability and sediment mobilization during the Bølling-Allerød periods (14.7 – 13 ka). Age control for future work should focus on features that are not dependent on local climate.

1 Introduction

Much glacial research over the last century has focused on the style and timing of Laurentide Ice Sheet (LIS) recession from the Great Lakes region of North America following the Last Glacial Maximum (LGM, 26-19 ka; Dalton et al., 2020; Dyke, 2004; Fairchild, 1909). Well constrained ice sheet chronologies are necessary to determine the timing of meltwater re-routing events from ice-dammed lakes that occupied the Great Lakes basins during the last deglaciation (Barth et al., 2019; Calkin and Feenstra, 1985; Leydet et al., 2018; Porreca et al., 2018; Rayburn et al., 2007), as these events are hypothesized to have had significant climatic impacts (Broecker et al., 1989; Donnelly et al., 2005). Models that attempt to understand past climate change (Osman et al., 2021), ice sheet sensitivity (Briner et al., 2020), and atmospheric organization (Löfverström et al., 2014; Tulenko et al., 2020) all require paleo ice sheet configurations. Therefore, well-defined ice sheet retreat chronologies are critical for understanding dynamics and forcings within the late glacial climate system.

Despite the critical need for precise chronologies of ice margin retreat of the LIS in the Great Lakes region, ice margin reconstructions in western New York lack detailed age control. Here, there are no local ages on the

terminal moraine and few from the recessional moraines (Muller and Calkin, 1993), leaving the deglacial

chronology to be largely based on correlations with dated moraines and proglacial shorelines to the west in Ohio and

to the east in New York (Fullerton, 1980; Ridge, 2003). These correlations suggest that the western New York Kent

(terminal) and Lake Escarpment (recessional) moraines date to ~20 and 17 ka, respectively (Fig. 1). However,

Young et al. (2020) recently interpreted new and existing radiocarbon ages from western New York to support a re-

advance of the LIS ~13 ka that overtopped the Lake Escarpment Moraine and nearly reached the Kent Moraine (Fig.

1). The evidence includes the re-interpretation of several unrelated sites throughout western New York, but largely

hinges on new trenched sediment sections near the Kent Moraine revealing logs in clayey diamicton, which Young

et al. (2020) suggest requires glacial overriding of a forest ~13.3 to 13.0 ka. In contrast to Young et al.'s (2020)

reconstruction, most literature places the LIS margin north of Lake Ontario at this time (Dalton et al., 2020; Muller

and Calkin, 1993; Terasmae, 1980; and references therein), with the drainage of Glacial Lake Iroquois occurring at

~13 ka (Fig. 1; Cronin et al., 2012; Lewis and Anderson, 2019; Rayburn et al., 2005). To reconcile the disagreement

in timing between the hypothesized re-advance and existing chronologies, Young et al. (2020) invoke a largely

floating ice mass that left minimal traces of its existence in most areas. If a re-advance of the scale hypothesized by

Young et al. (2020) occurred (henceforth referred to as the 'Allerød re-advance hypothesis'), there would be a need

to revisit many regional deglaciation chronologies.

To further constrain moraine ages in western New York and to test the Allerød re-advance hypothesis, we

obtained 23 new macrofossil-based radiocarbon ages from five sediment cores collected on the Kent Moraine, and

18 new macrofossil-based radiocarbon ages from two sediment cores on the Lake Escarpment Moraine. The Lake

Escarpment Moraine is within the extent of the proposed re-advance, so if basal ages from sites on this moraine pre-

date ~13 ka, and the subsequent stratigraphy shows no evidence of a re-advance, then the evidence would refute the

Allerød re-advance hypothesis. Conversely, basal radiocarbon ages that post-date ~13 ka, and/or evidence that the

sediment stratigraphy is interrupted at ~13 ka, would support an Allerød re-advance. Additionally, we obtained two

optically stimulated luminescence (OSL) ages from kame delta sediments associated with deposition of the Kent

Moraine to provide a more complete understanding of deglaciation. Our results provide new chronological

constraints in the western New York data gap, and do not support the ~13 ka re-advance proposed by Young et al.

(2020). Rather, our data support a model of initial moraine deposition followed by thousands of years before kettle

basin formation and final moraine stabilization.
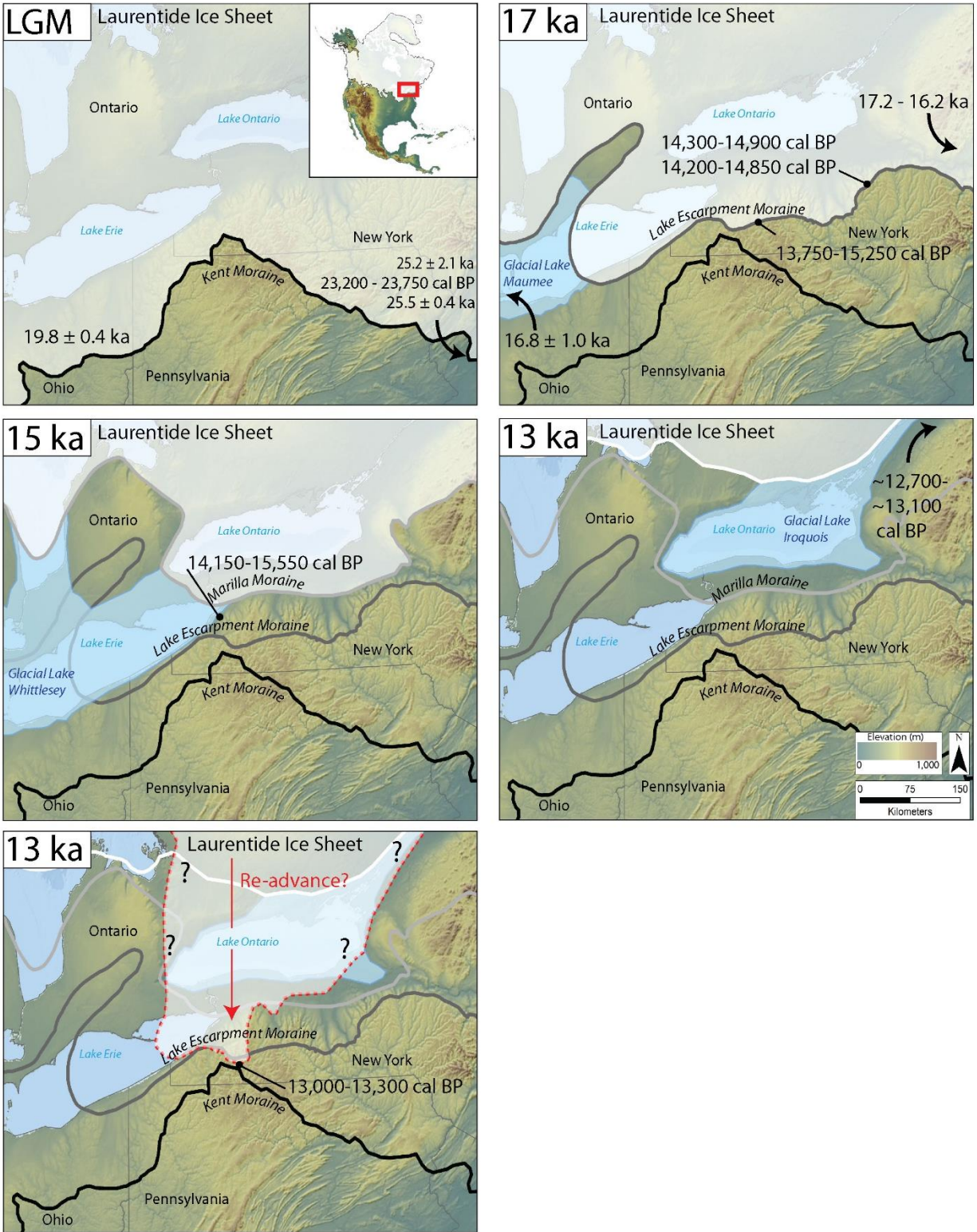
78
79 **Figure 1. Map depictions of the deglaciation of the eastern Great Lakes after the Last Glacial Maximum. Black line is the**
80 **Kent Moraine, modified from Dalton et al. (2020), the 'Pennsylvania Department of Conservation and Natural Resources**
81 **Late Wisconsin Glacial Border' (https://www.pasda.psu.edu), and the 'Quaternary Geology 500K - Glacial Boundary of**
82 **Ohio' (https://gis.ohiodnr.gov). Dark gray line is the 17 ka ice margin from Dalton et al. (2020) which depicts the Lake**
83 **Escarpment Moraine. Light gray line is the 15 ka ice margin from Dalton et al. (2020) which depicts the Marilla Moraine.**

84 **Glacial Lake Maumee and Whittlesey are included for general reference, and drawn with shoreline elevations (Fisher et**
85 **al., 2015). White line is the 13 ka ice margin from Dalton et al. (2020) and we estimated Glacial Lake Iroquois using Bird**
86 **and Kozlowski (2016). Red dashed line depicts a hypothesized ice sheet configuration to explain the hypothesis presented**
87 **in Young et al. (2020). Note that the LIS would dam a pro-glacial lake in the Lake Erie basin and overrun several moraine**
88 **belts, including the Lake Escarpment Moraine. Radiocarbon, cosmogenic nuclide, and OSL ages discussed in the text are**
89 **shown with approximate locations. Arrows indicate study sites are off the map extent. Panel LGM: Glover et al. (2011),**
90 **Corbett et al. (2017), Stanford et al. (2020), Balco et al. (2009), and Balco et al. (2002). Panel 17 ka: Fisher et al. (2015), Fritz**
91 **et al. (1987), Kozlowski et al. (2018), and Ridge (2003). Panel 15 ka: Calkin and McAndrews (1980). Panels 13 ka: Lewis**
92 **and Anderson (2019), Rayburn et al. (2007), Richard and Occhietti (2005), and Young et al. (2020). DEM from U.S.**
93 **Geological Survey's Center for Earth Resources Observations and Science (EROS).**

94

2 Geologic Setting

96   The Kent Moraine in western New York is correlated to the Kent Moraine in northwest Ohio, the Olean
97 Moraine in Pennsylvania, the Harbor Hill Moraine in New Jersey, and the Martha's Vineyard Moraine in
98 Massachusetts (Fig. 1; Balco et al., 2002; Fullerton, 1980; Muller and Calkin, 1993; Stanford et al., 2020). Retreat
99 from the LGM moraine in these adjacent regions is dated to 19.8 ± 0.4 ka in Ohio (Glover et al., 2011), 25.2 ± 2.1 ka
100 (Corbett et al., 2017) and 23,200-23,750 cal BP in New Jersey (Stanford et al., 2020), and 25.5 ± 0.4 ka in
101 Massachusetts (Balco et al., 2009; Balco et al., 2002). Therefore, we infer that the Kent Moraine in western New
102 York was likely deposited sometime between 25 and 20 ka.
103   The first major moraine belts deposited after the maximum LGM position were the Ashtabula Moraine in
104 Ohio and northwest Pennsylvania, the Lake Escarpment Moraine in western New York, and Valley Heads moraines
105 in central New York (Fig. 1; Fullerton, 1980; Muller and Calkin, 1993). During this ice position, Glacial Lake
106 Maumee occupied the Lake Erie basin around 17,000 - 16,000 cal BP based on radiocarbon dating at the paleo-
107 outlet and OSL dating of strandlines (Calkin and Feenstra, 1985; Eschman and Karrow, 1985; Fisher et al., 2015).
108 Ridge (2003) tied the outer and inner Valley Heads moraines to the New England Varve Chronology, placing these
109 moraines at 17,200 and 16,200 cal BP, respectively. Kozlowski et al. (2018) report basal ages of 14,300-14,900 and
110 14,200-14,850 cal BP from basins within the outer Valley Heads limit. These ages are younger than previous
111 estimates, leading Kozlowski et al. (2018) to suggest the moraine may have been re-occupied. Fritz et al. (1987)
112 report minimum-limiting radiocarbon ages of 13,750-15,250 cal BP from wood within lake deposits stratigraphically
113 above outwash sands from Nichols Brook in western New York (Fig. 2). Muller and Calkin (1993) extrapolated
114 their ages to estimate ~17,600 cal BP for the emplacement of the outwash.
115   Following the deposition of the Lake Escarpment Moraine, Glacial Lakes Whittlesey and Warren occupied
116 the Lake Erie basin between 16 and 14 ka (Fig. 1; Fullerton, 1980; Muller and Calkin, 1993). The lowering of
117 Glacial Lake Whittlesey to Glacial Lake Warren is dated to 14,150-15,550 cal BP at Winter Gulf in western New
118 York (Fig. 2; Calkin and McAndrews, 1980), and Warren strandlines in northwest Ohio have been dated to $14.2 \pm$
119 1.3 ka (Higley et al., 2014) and 14.1 ± 1.0 ka in (Campbell et al., 2011). These proglacial lake chronologies provide
120 unambiguous minimum age constraints of >15 ka for the deposition of the Lake Escarpment Moraine.
121   The LIS continued its northward retreat and formed Glacial Lake Iroquois from 14.7 to 13.0 ka in the Lake
122 Ontario basin (Fig. 1; Muller and Calkin, 1993; Muller and Prest, 1985; Teller, 2003). The switch of the Glacial

123 Lake Iroquois spillway from the Mohawk River valley to the lower outlet at Covey Hill is constrained between

124 13,200 and 13,000 cal BP by numerous radiocarbon constraints from the pre- and post-flood histories of Lake

125 Vermont and Lake Iroquois (Lewis and Anderson, 2019; Rayburn et al., 2007; Richard and Occhietti, 2005).

126 Similarly, the formation of the Champlain Sea occurred between 13,100 and 12,700 cal BP, which post-dates the

127 final draining of Glacial Lake Iroquois and requires an ice margin north of the Lake Ontario outlet (Cronin et al.,

128 2012; Rayburn et al., 2011). Collectively, this ice recession chronology is at odds with the Allerød re-advance

129 hypothesis, with its LIS advance across the Lake Ontario basin and to near the terminal moraine in western New

130 York ~13 ka (Fig. 1; Young et al., 2020).
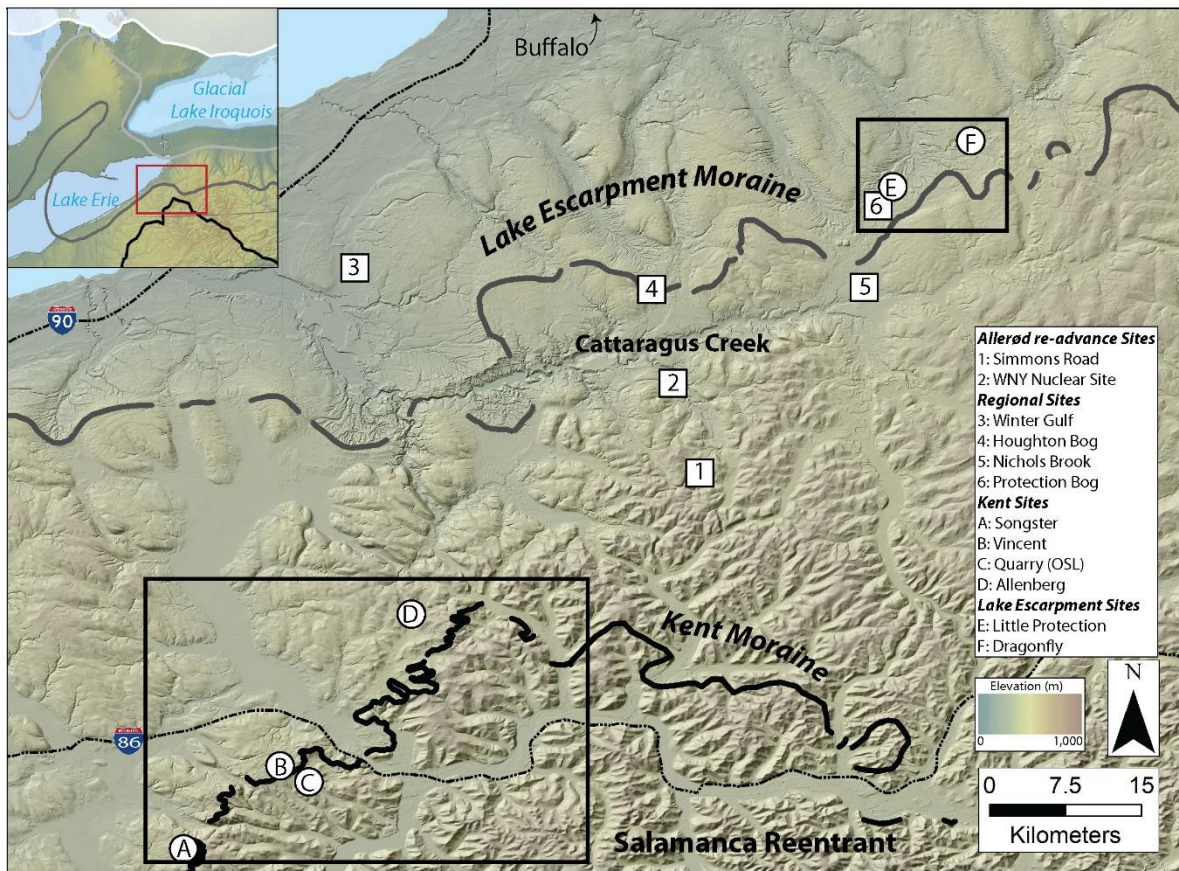
131

132 **Figure 2. Study sites in relation to previously published work. Black and gray lines are the same as in Fig. 1. Squares 1 and**
133 **2 depict hypothesized sites overrun by the Allerød re-advance at 13 ka (Young et al., 2020). Circles A-D are our sites on the**
134 **Kent Moraine. Circles E and F are our sites on the Lake Escarpment Moraine. Squares 3-6 are Winter Gulf and Nichols**
135 **Brook (Calkin and McAndrews, 1980), and Houghton and Protection Bog (Miller, 1973). The two black boxes show the**
136 **extent of the maps in Fig. 3. DEM from U.S. Geological Survey's Center for Earth Resources Observations and Science**
137 **(EROS).**

138

3 Methods

3. 1 Sediment cores

Our primary approach for constraining the timing of deglaciation and testing the Allerød re-advance hypothesis was obtaining basal sediment ages from kettles within the Kent and Lake Escarpment Moraines. Newly available light detection and ranging (LiDAR)-based bare-Earth 1-m digital elevation models (DEMs) enabled us to identify natural kettle basins (Fig. 3). Typically, moraines in western New York have both single ridges where the ice sheet abutted higher topography, and hummocky moraine belts that contain numerous kettle basins. Kame deltas exist in places where the ice sheet dammed adjacent river valleys. The hummocky nature of most moraines indicates that the moraines were ice-rich when deposited (Fig. 3).

We collected sediment cores from kettles that presently range from bogs to wetlands. We cored five sites on the Kent Moraine referred to as the Vincent-1 (core name: 20VIN1), Vincent-3 (20VIN3), Vincent-4 (20VIN4), Songster (21SONG1), and Allenberg (15ABB7) sites (Table 1, Fig. 3), and two sites on the Lake Escarpment Moraine referred to as the Little Protection (21LPB1) and Dragonfly (13DFK1) sites (Table 1, Fig. 3). All sites are within hummocky moraine.

We determined basin depocenters using thin steel rods to measure the depth of the organic sediment infill. In the depocenter, we used Livingstone- and Russian Peat-style corers to collect organic-rich sediment infill, and a manual percussion GeoProbe system to collect the underlying stiff, minerogenic sediments. From some sites, our sediment cores extended from the present surface to mineral-rich sediments below the organic-sediment infill; from others, our sediment cores began and ended at depth, spanning the organic-to-mineral sediment contact and downward until we penetrated coarse deposits (Table 1). We returned and cored the Vincent-1 and -4 sites multiple times to collect the entire sequence.

We split, imaged, and generated downcore data on all sediment cores at the University at Buffalo. We measured magnetic susceptibility in contiguous 1 cm intervals using a Bartington MS2E High Resolution Surface Scanning Sensor scanner connected to a Bartington MS2 Magnetic Susceptibility Meter to assess the minerogenic content. We calculated loss-on-ignition (LOI) percent by burning ~1 cm^3 of sediment in a Thermolyne Muffle Furnace at successively higher temperatures for water (105°C), organic carbon (550°C), and carbonate (950°C) content to help characterize the sediment units and depositional setting (Heiri et al., 2001; Last and Smol, 2001). To calculate composite core length, we spliced together overlapping sediment sections using visual lithologic changes and magnetic susceptibility measurements. We volumetrically sampled portions of the Little Protection sediment cores to determine sediment bulk density; these data are used to check for overcompaction during an Allerød re-advance. The data are only from Little Protection because Dragonfly data creation took place previous to Young et al. (2020) and we did not measure bulk density.

We use radiocarbon dating of macrofossils for age control (Table 2). The sediments are organic-rich in the upper portions of the cores and are organic-poor in the lower sections. Where available, we picked full plant macrofossils. We picked macrofossils that were from the center of the sediment core and demonstrably in-situ. In macrofossil-devoid sections, we wet sieved sediment with deionized water to isolate and combine the largest

175 macrofossil fragments for dating. We attempted to identify macrofossils, but some macrofossil fragments were small
176 and unidentifiable (Table 2). We rinsed samples with deionized water, freeze-dried them, and sent samples to the
177 National Ocean Sciences Accelerator Mass Spectrometry (NOSAMS) or the Keck Lab at the University of
178 California Irvine (KCCAMS) for radiocarbon analysis. The facilities conducted acid-base-acid (ABA)
179 pretreatments, converted samples to graphite, and ran them on the AMS (Elder et al., 2019; Olsson, 1986; Pearson et
180 al., 1997; Shah Walter et al., 2015; Vogel et al., 1984).
181 In Table 2, we report the 2σ age range and round ages according to Stuiver and Polach (1977). We
182 calibrated all the radiocarbon results using Calib8.1 with the IntCal20 dataset (Reimer et al., 2020; Stuiver and
183 Reimer, 1993). All radiocarbon ages in the text were recalibrated with IntCal20. $\delta^{13}C$ measurements were measured
184 on a split of the CO_2 gas generated from each sample on an isotope-ratio mass spectrometer. Uncertainties in the
185 $\delta^{13}C$ from both labs are <0.1‰. We report $\delta^{13}C$ values as ‰ VPDB.
186

Table 1: Site location, core lengths, and ownership.

Site Name	Core Name	Latitude (DD)	Longitude (DD)	Elevation (m asl)	Site Length (m)	Core Top (m bg)	Core Bottom (m bg)	Property Ownership
Vincent 1	20VIN1	42.109	-79.000	596	145.0	0.0	6.6	Vincent Family
Vincent 3	20VIN3	42.110	-78.999	593	39.0	1.5	2.9	Vincent Family
Vincent 4	20VIN4	42.109	-78.999	594	81.0	3.1	5.4	Vincent Family
Songster	21SONG1	42.040	-79.079	581	172.0	4.1	4.8	Songster Family
Allenberg	15ABB7	42.252	-78.883	524	321.0	8.0	14.6	Buffalo Audubon Society
Little Protection	21LPB1	42.621	-78.463	440	228.0	0.0	8.1	Erie County Parks Dept.
Dragonfly	13DFK1	42.679	-78.386	450	117.0	0.0	7.3	Buffalo Audubon Society
Corbett Hill	-	42.114	-78.946	530	-	-	-	JMI Corbett Hill Gravel

DD: Decimal Degrees
asl: Above sea level
bg: Below ground

187

188
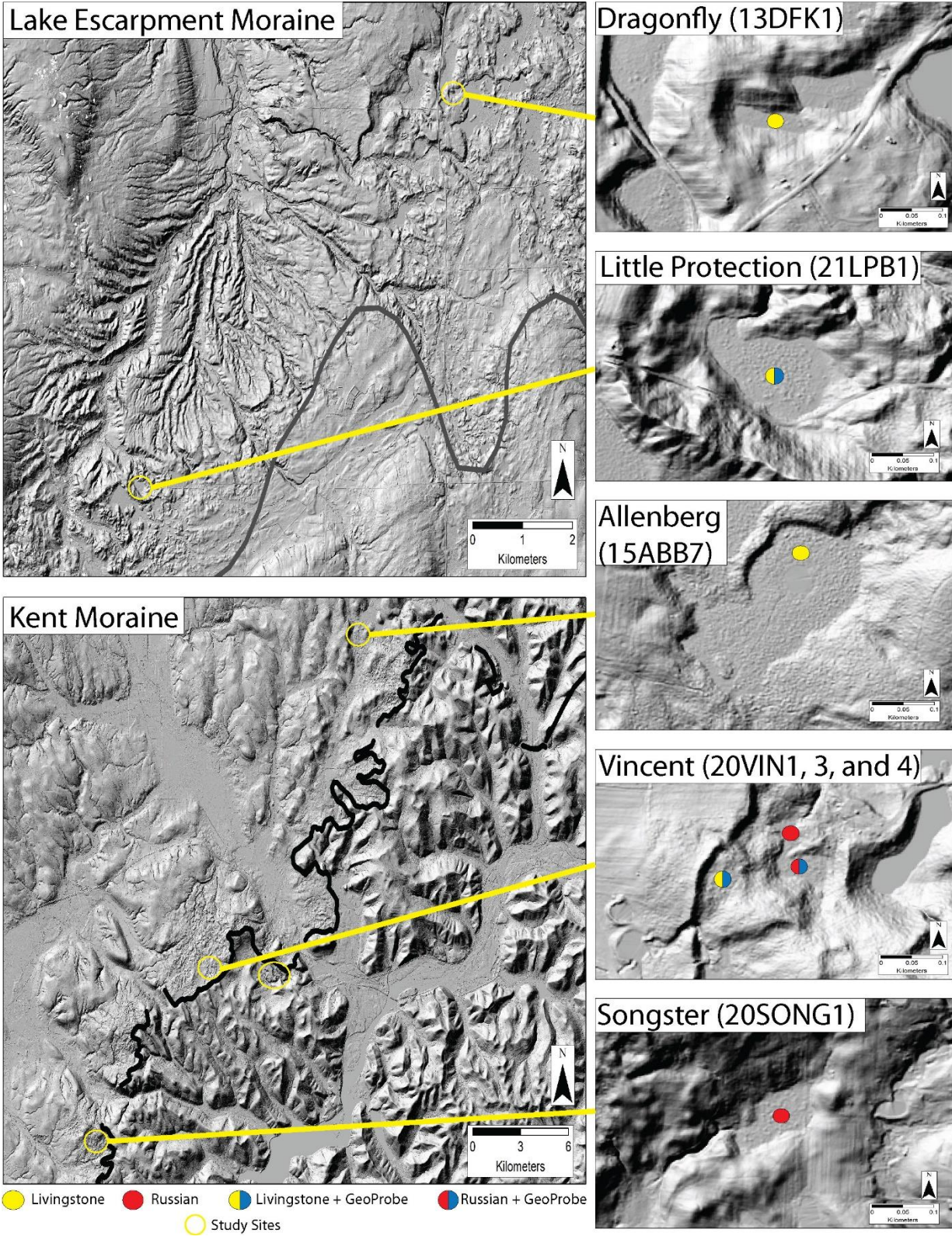
Figure 3. Site maps of the sediment core locations. 1-m bare-Earth DEM hillshade from https://data.gis.ny.gov/ with the
Kent (black) and Lake Escarpment (gray) moraines. Open yellow circles depict study site location and yellow lines associate
each site location with a site map. Figure 4 contains the site map for the open yellow circle with no associated site map. The

196

3.2 Optically stimulated luminescence dating

198 We collected sediment samples for OSL dating from topset beds within an ice-contact delta deposit
199 associated with the Kent Moraine to determine when the LIS was present at this location (Fig. 3 & 4). Our sample
200 location was Corbett Hill Gravel Quarry, an active aggregate quarry that exposes large sedimentary sequences
201 indicative of a proglacial delta. The sediments consisted of cobble-rich foreset beds overlain by ~3 m of near-
202 horizontal topset beds. We collected sand samples for OSL dating from the topset sequence ~2.1 m below the delta
203 surface. We created a fresh exposure of the topset beds with an excavator, exposing alternating layers of gravels and
204 coarse sands, with lenses of medium/fine-sand and silt. We collected two samples for OSL dating in fine-sand lenses
205 in 5.1 x 25.4 cm (2 x 10 inch) aluminum tubes after clearing back outer sediments (Fig. 4). Samples for water
206 content and dose rate determination were collected from surrounding sediments.

207 We processed the samples at the Utah State University Luminescence Laboratory for small aliquot OSL
208 dating of fine-grained quartz sand (Table 3, Table S1). First, we purified samples to 150-250 μm quartz sand using
209 wet sieving, and chemical treatment with 10% hydrochloric acid to remove carbonates, 5% peroxide to remove
210 organics, 2.72 g/cm^3 sodium polytungstate to remove heavy minerals and 48% hydrofluoric acid to remove feldspars
211 and etch the quartz grains. We analyzed small aliquots of quartz (0.4 to 1 mm diameter of sand mounted on disk,
212 ~10-20 grains) on Risø DA-20 readers, using the single-aliquot regenerative-dose (SAR) protocol (Murray and
213 Wintle, 2000). We analyzed 42 aliquots for sample 21SICK-01 and 37 for sample 21SICK-02, of which we used 21
214 and 23 aliquots for age calculations, respectively (Fig. 4 & S7). Aliquots were rejected from age calculation if they
215 showed signal depletion with infrared stimulation indicating feldspar contamination (0-12 aliquots), poor recycling
216 of a repeat point (greater than 80% difference between repeat points, 7-8 aliquots), high recuperation of a zero-dose
217 point (>10% of the Natural signal, 0-6 aliquots), extrapolation of the equivalent dose beyond the dose-response
218 curve (0-2 aliquots) and poor dose-response curve fit (0-3 of aliquots). We applied a minimum age model (MAM) to
219 the samples to calculate our equivalent does (D_E; Grays; Gy, Fig. 4 & S7), as used by similar studies on LIS
220 glaciofluvial terraces elsewhere in the northern United States (Rittenour et al., 2015). MAMs are useful in these
221 glaciofluvial environments because of the increased potential for incomplete bleaching from subglacial or turbid
222 water sediment transport.

223 We determined the dose rate for OSL age calculation based on U, Th, K, and Rb concentrations from the
224 surrounding sediments using inductively coupled plasma-mass spectrometry and atomic emission spectrometry.
225 Using the conversion factors of Guérin et al. (2011), we converted elemental concentrations to dose rate. The
226 contribution of cosmic radiation was based on sample depth, elevation and latitude following Prescott and Hutton
227 (1994). We also determined water content by measuring the mass of the samples before and after desiccation. With
228 these three factors, we were able to calculate environmental dose rates (Gy/kyr). Our reported OSL ages are simply

229   the D_E (determined with the MAM) divided by the dose rate with 1σ standard error (Table 3). We report ages with

230   1σ uncertainty (Table 3).
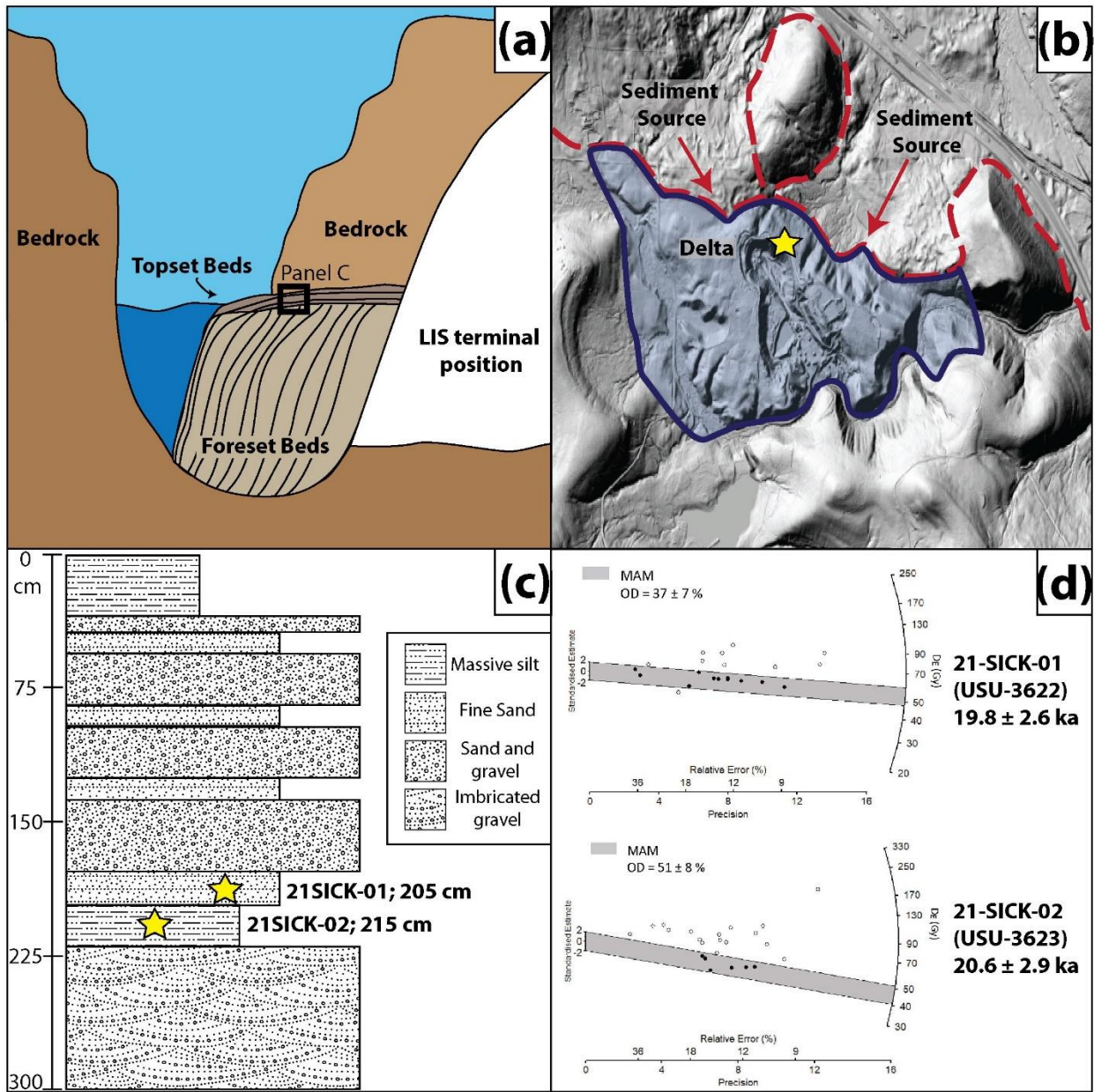
231

232   **Figure 4. Panel A) is a schematic of the kame delta creation. The LIS dammed a lake and deposited the delta outboard of**
233   **the Kent Moraine. B) is a 1-m DEM hillshade showing the kame delta outboard of the Kent Moraine (within the open yellow**
234   **circle in Fig. 3). Red dashed line depicts the extent of the Kent Moraine. Red arrows depict the sediment source for the**
235   **delta. Blue line and shading depicts the delta deposit. Yellow star on the side of the active quarry shows our sampling site.**
236   **C) shows a stratigraphic column of the topset beds. We use the FGDC Digital Cartographic Standard for Geologic Map**
237   **Symbolization (U.S. Geological Survey). Yellow stars show our sampling location. D) Equivalent dose (D_E) distributions for**
238   **the luminescence samples collected from the kame delta associated with an ice-margin position near the Kent moraine.**
239   **MAM = minimum age model of Galbraith and Roberts (2012) fit to the D_E data (gray shaded region). OD = overdispersion,**
240   **a metric of D_E scatter beyond instrumental error, where OD > 30% is interpreted to be due to partial bleaching due to**
241   **incomplete solar resetting of the luminescence signals in the quartz grains.**

242

4 Results

4.1 Stratigraphy and Radiocarbon Results

Vincent-1 (Kent Moraine)

The bottom 2.5 m is a gray massive pebbly diamicton with a silty matrix that we call Unit 1. We only recovered Unit 1 at this study site and collected it with the Geoprobe system (Fig. 5). There is a sharp contact with layered gray sand and silt that grades to alternating massive brown and gray silt with sparse macrofossils. We call this Unit 2. There is a sharp contact with massive dark brown organic-rich silt that we call Lower Unit 3. In the initial sediments of Lower Unit 3, there are three layers of gray silt and an inclusion of gray clay that are identical to the sediment of Unit 2. There is a sharp contact with peat which continues to the top of the core that we call Upper Unit 3. Broadly, this sediment progression is found in the other six sediment cores from both moraines, so we use Unit 2 and 3 terminologies for them as well. Figures 5a and 5b depict the downcore data. For all seven sediment cores, magnetic susceptibility values are higher in Unit 2 than Unit 3, water and organic carbon content values are lowest in Unit 2, rise in Lower Unit 3, and are highest in Upper Unit 3, and calcium carbonate remains below 8% in all sediment cores so it is not plotted in Fig. 5.

Figure 5 and Supplementary Figure 1 show the ten radiocarbon ages from 20VIN1. The seven ages in Unit 2 are from combined macrofossils and have little stratigraphic order. The three ages in Unit 3, from single macrofossils, are in stratigraphic order. 20VIN1 has an age of 15,050-15,550 cal BP from the bottom of Unit 2, yet is stratigraphically below older ages from Unit 2 of 15,650-15,900, 15,800-16,150, and 16,050-16,300 cal BP. There is an inclusion of macrofossils at the Unit 2/3 contact that was dated twice and yields two radiocarbon ages from combined macrofossils of 19,350-19,600 and 14,050-14,850 cal BP; combined macrofossils from the surrounding sediment produce an age of 14,300-15,050 cal BP. *Picea* seeds from the top of Lower Unit 3 are 13,650-14,050 cal BP. There are two ages in the Upper Unit 3; a twig that dates to 13,150-13,300 and wood that dates to 8,390-8,520 cal BP.

Vincent-3 (Kent Moraine)

In 20VIN3, Unit 2 begins as gray silt, transitions to a light brown silt, and is topped by gray clay. The contact with Unit 3 is sharp. Unit 3 is massive organic-rich silt. There is a layer of gray silt in the base of Unit 3. There are two radiocarbon ages from 20VIN3 (Fig. 5; Fig. S2). The one age in Unit 2 is from combined macrofossils that date to 14,350 – 15,150 cal BP. The one age at the base of Unit 3 is from combined macrofossils and dates to 15,350 – 15,650 cal BP.

Vincent-4 (Kent Moraine)

In 20VIN4, Unit 2 contains alternating layers of pebbly diamicton (with some clasts up to 5 cm long) and silty clay. The contacts between the layers are sharp and one is undulating. Unit 3 is a massive organic-rich silt.

275   There are four radiocarbon ages from Unit 2 (Fig. 5; Fig. S3). The lowest age is from a piece of wood that dates to

276   14,250 – 15,000 cal BP. Then the next three ages are from combined macrofossils and date to 14,150 – 14,850,

277   14,300 – 14,900, and 14,300 – 14,900 cal BP.

Songster (Kent Moraine)

279   In 21SONG1, Unit 2 is silty clay with pebbles. The contact with Unit 3 is sharp. Unit 3 begins with

280   organic-rich silt with some sand and pebbles. Large macrofossils are common. This grades into organic-rich silt.

281   One radiocarbon age from a piece of wood in the bottom of Unit 3 dates to 14,350 – 15,050 cal BP (Fig. 5).

Allenberg (Kent Moraine)

283   In 15ABB7, we did not collect Unit 2. Lower Unit 3 is an organic-rich silt and Upper Unit 3 is peat. There

284   are four ages from Unit 3 (Fig. 5; Fig. S4). These samples were not identified at the time of dating. The lowest age is

285   13,800 – 14,050 cal BP. The next 3 ages are in stratigraphic order and range from 12,700 – 12,850 to 795 – 920 cal

286   BP.

Little Protection (Lake Escarpment Moraine)

288   In 21LPB1, Unit 2 begins with 2 cm of gray silty gravel before a sharp contact with massive, oxidized sand

289   and gravel. Above this is a sharp transition to alternating layers of gray silt, silty gravel, and sand; these layers have

290   sharp and sometimes undulating contacts. That is overlain by massive gray clay. The contact with Unit 3 is gradual

291   over 3 cm. Lower Unit 3 is an organic-rich silt and Upper Unit 3 is peat. There is one radiocarbon age from Unit 2

292   on a fish bone that dates to 16,650 – 17,350 cal BP. There are eight radiocarbon ages from Unit 3 (Fig. 5; Fig. S6).

293   The lowest age is from a piece of wood that dates to 13,600 – 14,000 cal BP. The next seven are in stratigraphic

294   order and range from 13,350 – 13,600 to 5,580 – 5,650 cal BP. To address the Allerød re-advance hypothesis and

295   seek evidence of whether the coring sites were overridden, we measured dry bulk density at 1-cm-resolution through

296   the time interval of hypothesized re-advance. The bulk density decreases from 1.55 g/cm^3 to 0.42 g/cm^3 in the

297   transition from Unit 2 to 3. (Fig. 5) The density decreases due to the transition from minerogenic silt to organic-rich

298   silt and remains below 0.42 g/cm^3 into Unit 3.

Dragonfly (Lake Escarpment Moraine)

300   In 13DFK1, Unit 2 is gray silt. The contact with Unit 3 is sharp. Lower Unit 3 is an organic-rich silt and

301   Upper Unit 3 is peat. There are nine radiocarbon ages from Unit 3 (Fig. 5; Fig. S5). The lowest age is from grass and

302   dates to 15,000 – 15,400 cal BP. The next eight radiocarbon ages are in stratigraphic order and range from 13,800 –

303   14,000 to 4,420 – 4,800 cal BP.

304

306

307
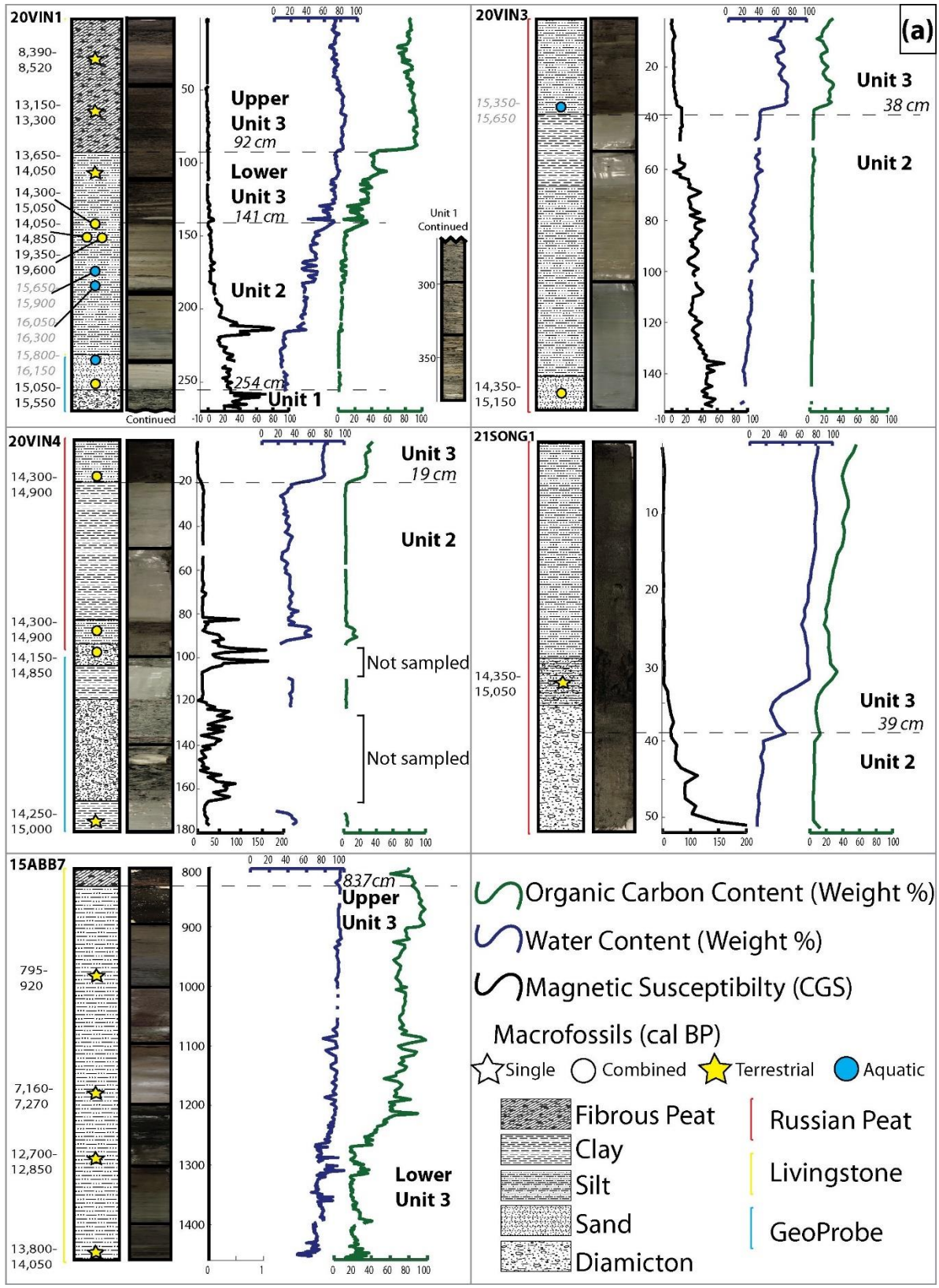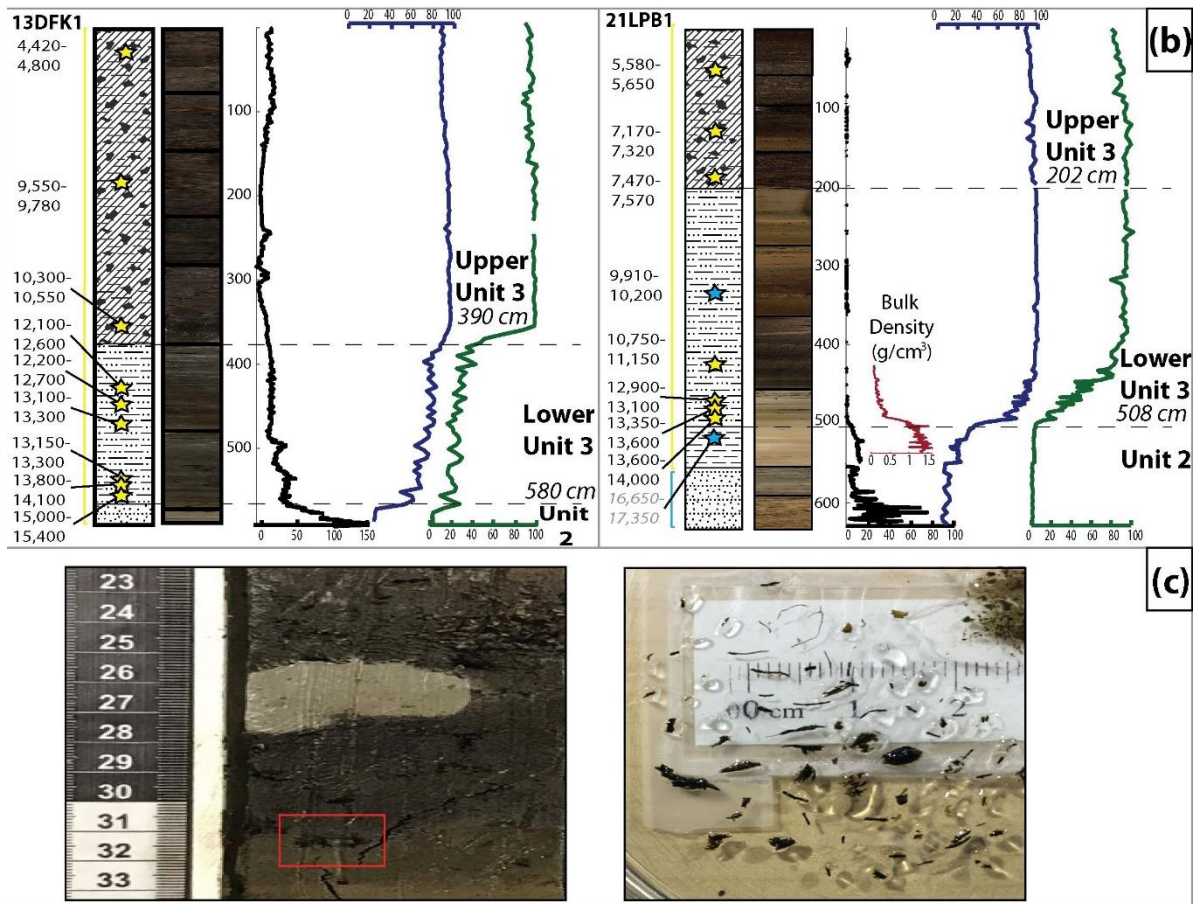
Figure 5. Panel A) has the sediment core stratigraphy from the Kent Moraine sites, and B) has the sediment core stratigraphy from the Lake Escarpment Moraine sites. We show sediment texture next to the core images using the FGDC Digital Cartographic Standard for Geologic Map Symbolization (U.S. Geological Survey). We plot magnetic susceptibility (CGS; black line), water content (weight %; blue line), and organic content (weight %, green line) by composite depth (cm). The colored line next to the stratigraphic column depicts if we used the Russian Peat Corer (red), Livingstone Corer (yellow), or GeoProbe (blue). Stars indicate single macrofossils and circles indicate when we combined macrofossils. The yellow filling indicates the sample is terrestrial and blue indicates the sample has aquatic macrofossils within it. Radiocarbon ages presented as the full 2σ range in cal BP. We used gray text and italics for radiocarbon ages we suspect have hardwater contamination. C) is a close-up image of the inferred gray clay and macrofossil-rich rip-up clasts in the transition from Unit 2 to 3 in 20VIN1 (shown in red box). The black box has post-sieve macrofossils from the rip-up clast in the red box.

319

320

321

322

323

Table 2: Radiocarbon dates for each study site. Listed by depth.

Lab Code	Depth (cm)	Material Dated	Mass (mg)	$\delta^{13}C$‰	Fraction Modern	Fraction Modern Error	^{14}C (BP)	^{14}C error (BP)	2 σ age range (cal BP)	
Vincent-1 (20VIN1)										
OS-164770	27.3	Wood	5.8	-26.5	0.3854	0.0015	7,660	30	8,390 8,520	98%
OS-164771	67.3	Twig	5.8	-28.7	0.2441	0.0015	11,350	50	13,150 13,300	97%
OS-164772	109.5-111.0	*Picea* seeds	75.7	-23.0	0.2263	0.0016	11,950	55	13,650 13,700	6%
									13,750 14,050	91%
OS-164773	145.0	Unidentifiable	2.3	-24.3	0.2105	0.0016	12,500	60	14,300 14,750	56%
									14,750 15,050	44%
UCIAMS-239749	145.2	Moss, unidentifiable	2.4	-28.3	0.1342	0.0007	16,135	45	a19,350 19,600	100%
OS-164808	145.2	Moss, unidentifiable	2.4	-26.8	0.2169	0.0019	12,300	70	14,050 14,550	84%
									14,700 14,850	16%
UCIAMS-239748	181.0-182.5	*Drepanocladus, Paludella squarrosa, Potomegeton,* unidentifiable	6.8	-19.4	0.1949	0.0006	13,135	30	a15,650 15,900	100%
UCIAMS-239746	185.5-188.5	Moss, *Potomegeton,* unidentifiable	2.1	-14.6	0.1875	0.0006	13,450	25	a16,050 16,300	100%
UCIAMS-239745	239.0-241.5	Unidentifiable	2.5	NA	0.1910	0.0009	13,300	40	a15,800 16,150	100%
OS-162874	255.0	Moss, unidentifiable	2.5	-26.6	0.2029	0.0020	12,800	80	15,050 15,550	100%
Vincent-3 (20VIN3)										
UCIAMS-239753	34.5-35.5	*Chara,* unidentifiable	25.8	-15.3	0.1988	0.0006	12,980	25	a15,350 15,650	100%
OS-162873	146.5-152.0	Unidentifiable	2.1	-26.6	0.2100	0.0020	12,550	75	14,350 14,750	37%
									14,800 15,150	63%
Vincent-4 (20VIN4)										
UCIAMS-239752	17.0-18.0	Beetle wing, *Cladocera, Chara,* unidentifiable	5.1	-24.9	0.2126	0.0007	12,435	30	14,300 14,900	100%
UCIAMS-239751	87.0-88.0	Unidentifiable	39.2	NA	0.2127	0.0010	12,435	40	14,300 14,900	100%
UCIAMS-239750	97.5-98.8	Unidentifiable	6.3	NA	0.2150	0.0011	12,350	45	14,150 14,550	76%
									14,700 14,850	24%

continued

324

325

Lab ID	Depth	Material							Calibrated range		%
OS-162875	174.0–175.0	Twig	2.0	-28.0	0.2120	0.0019	12,450	75	14,250	15,000	100%
Songster (21SONG1)											
OS-160884	39.3	Bark (likely *Picea*)	6.4	NA	0.2107	0.0015	12,500	55	14,350	14,750	55%
									14,750	15,050	45%
Allenberg (15ABB7)											
OS-123347	971.0	Not identified	NA	-26.0	0.8877	0.0019	955	20	795	875	79%
									895	920	19%
OS-123426	1178.0	Not identified	NA	-27.1	0.4580	0.0018	6,270	30	7,160	7,270	96%
OS-123427	1295.0	Not identified	NA	-26.8	0.2607	0.0020	10,800	60	12,700	12,850	100%
OS-123348	1456.0	Not identified	NA	-24.6	0.2227	0.0012	12,050	40	13,800	14,050	100%
Little Protection (21LPB1)											
OS-163424	53.7	Wood	4.6	-24.6	0.5464	0.0014	4,860	20	5,580	5,600	89%
									5,640	5,650	6%
OS-163425	141.0	Wood	15.6	-28.3	0.4549	0.0017	6,330	30	7,170	7,220	44%
									7,240	7,320	56%
OS-163426	198.5	Wood	39.7	-28.0	0.4376	0.0013	6,640	25	7,470	7,570	96%
OS-163427	320.5	*Potomegeton*	5.4	-17.6	0.3295	0.0012	8,920	30	[a]9,910	10,100	66%
									10,100	10,200	34%
OS-163428	423.0	Seed pod	5.8	-28.0	0.3034	0.0015	9,580	40	10,750	11,100	99%
OS-163517	472.2	*Picea* cone	5.5	-25.7	0.2512	0.0016	11,100	50	12,900	13,100	100%
OS-163500	481.0	Wood	32.9	-27.0	0.2346	0.0017	11,650	60	13,350	13,600	100%
OS-163501	493.0	Wood	3.0	-27.3	0.2277	0.0015	11,900	55	13,600	13,850	89%
									13,950	14,000	11%
OS-163429	511.0	Fish bone	11.0	-26.5	0.1749	0.0023	14,000	110	[a]16,650	17,350	100%
Dragonfly (13DFK1)											
OS-106743	25.2	Twig	NA	-22.8	0.6025	0.0031	4,070	40	4,420	4,650	82%
									4,760	4,800	13%
OS-106745	194.9	Moss stems	NA	-26.6	0.3381	0.0016	8,710	40	9,550	9,780	95%
OS-106746	362.4	Moss stems	NA	-25.0	0.3157	0.0017	9,260	45	10,300	10,550	100%
OS-133658	431.5	Leaf	NA	-25.7	0.2729	0.0015	10,450	45	12,100	12,400	55%
									12,400	12,500	19%
									12,550	12,600	26%
OS-106747	453.5	Twig	NA	-25.9	0.2704	0.0017	10,500	50	12,200	12,250	5%

continued

326

OS-133659	482.5	Wood	NA	-25.6	0.2447	0.0016	11,300	50	12,250	12,300	6%
									12,300	12,350	4%
									12,450	12,700	84%
OS-106863	524.6	Twig	NA	-25.3	0.2428	0.0011	11,350	35	13,100	13,250	88%
									13,250	13,300	12%
OS-133660	541.6	Twig	NA	-25.7	0.2220	0.0015	12,100	55	13,150	13,300	100%
OS-107085	567.6	Grass	NA	-35.4	0.2048	0.0014	12,750	55	13,800	14,100	100%
									15,000	15,400	100%

[a] Samples not used in the discussion due to possible hardwater effect

NA: Not Available.

NA δ^{13}C: Sample was either too small or the measurement was not requested.

NA Mass: Not recorded

327

4.2 Optically stimulated luminescence dating

Our small-aliquot D_e results from both 21SICK-01 and -02 show evidence of partial bleaching, as expected in a glaciofluvial environment (Table 3; Fig. 4 & S7; Rittenour et al., 2015). D_e results from the two samples are considerably scattered, positively skewed, and have overdispersion values between ~30 and ~60%, all indicative of incomplete bleaching and justify the use of the MAM (e.g., Olley et al. (1999)). Our two OSL MAM ages are 19.8 ± 2.6 and 20.6 ± 2.9 ka. The two samples are from within 10 cm of each other and yield statistically indistinguishable ages.

Table 3. Optically Stimulated Luminescence Age Information

Sample num.	USU num.	Depth (m)	Num. of Analyses[1]	Dose Rate (Gy/kyr)	Equivalent Dose[2] ± 2σ (Gy)	OSL Age ± 1σ (ka)
21-SICK-1	USU-3622	2.05	21 (42)	2.70 ± 0.11	53.55 ± 11.51	**19.82 ± 2.60**
21-SICK-2	USU-3623	2.15	23 (37)	2.23 ± 0.09	46.09 ± 10.07	**20.63 ± 2.91**

[1] Age analysis using the single-aliquot regenerative-dose procedure of Murray and Wintle (2000) on 0.4-1-mm small-aliquots (SA) of quartz sand (150-250 μm). Number of aliquots used in age calculation and number of aliquots in parentheses.

[2] Equivalent dose (D_E) calculated using the Minimum Age Model (MAM) of Galbraith and Roberts (2012).

5 Discussion

5.1 Stratigraphy

We interpret Unit 1 as the primary till that comprises the Kent Moraine. At the Vincent-1 (20VIN1) site we cored from 4.1 to 6.6 m below the wetland surface (2.5 m), but only recovered 1.2 m due to compaction with the GeoProbe system. We assume we reached below the post-glacial infill and into the primary glacial deposit since this unit spans 2.5 m and we found no changes in stratigraphy (Fig. 5).

Given the hummocky nature of the moraines (Fig. 3), the complex stratigraphy within Unit 2 (Fig. 5), and the similarity between Unit 2 from all sediment cores, we interpret this unit to record the transition from an ice-cored moraine to the modern kettled topography for both moraines. The most striking feature of Unit 2 are the numerous transitions between fine- and coarse-grained deposition. We interpret Unit 2 silt and clay as being settled out of suspension in lacustrine conditions, indicating that all seven basins likely held small kettle lakes of shifting dimension during this period. We propose that the alternating clay and diamicton sediments captured in 20VIN4, on the Kent Moraine, are slumps of primary till into the kettle lake with otherwise clay-rich sedimentation; these slumps potentially occurred as buried glacial ice melted and destabilized the basin's slopes. The stratigraphy of Unit 2 in 21LPB1, on the Lake Escarpment Moraine, is likely the result of similar processes.

The transition in sediment type between Units 2 and 3 likely reflects a shift to more vegetation growing in the lake and landscape, in concert with increased stabilization of the surrounding moraine. We infer the minerogenic

355   sediments in the transition zone (inclusions of gray clay and brown silty macrofossils in 20VIN1) are rip-up clasts

356   by their clast-like appearance and stark contrast to the surrounding sediment (Fig 5; Panel C). They were potentially

357   frozen during the time of deposition. This suggests the presence of reworked material near the Unit 2/3 transition.

358   The subsequent transition from lacustrine organic-rich silt to peat (Lower and Upper Unit 3, respectively) records

359   the shift from lake to bog/wetland due to the filling of the basin, shallowing of the lake, and encroachment of the

360   shoreline.

361

5.2 Chronology

363   The OSL samples are from 2 m below the surface of the ~70 m thick kame delta. The sample location

364   within the topset beds of a short-lived ice-contact delta suggests that our OSL samples constrain the time just before

365   the ice sheet retreated and ceased building the delta $19.8 \pm 2.6 - 20.6 \pm 2.9$ ka. The OSL ages support the estimated

366   age of 25 – 20 ka for the Kent Moraine from prior literature and affirms our confidence in the age assignments using

367   correlations of dated features elsewhere (Balco et al., 2009; Balco et al., 2002; Corbett et al., 2017; Glover et al.,

368   2011; Stanford et al., 2020).

369   We have identified spores and seeds of aquatic plants *Chara* and *Potamogeton* (O. Bennike, personal

370   communication) among the macrofossils from samples dating to 15,800 - 16,150, 16,050-16,300 and 15,650-15,900

371   cal BP from 20VIN1 and the sample dating to 15,350-16,650 cal BP from 20VIN3. These macrofossil samples also

372   have enriched δ^{13}C values, suggesting they contained aquatic material (except 15,800 - 16,150, which was too small

373   for a δ^{13}C measurement; Deuser and Degens, 1967; Oana and Deevey, 1960; Wang and Wooller, 2006). Our sites lie

374   within calcareous tills that overlie sedimentary bedrock (LaFleur, 1979; MacClintock and Apfel, 1944), which can

375   add aged carbon to the lake water. Aquatic plants derive their carbon from lake water, so radiocarbon ages from

376   aquatic plants could produce radiocarbon ages that overestimate the age of the material (the 'hardwater effect';

377   Deevey et al., 1954; Keeley and Sandquist, 1992). The lowest sample in 21LPB1 is from a fish bone (16,650 -

378   17,350 cal BP); a fish could be susceptible to the same hardwater effect as aquatic vegetation, and thus we do not

379   use it in our evaluation. We move forward using samples assumed to be terrestrial from a lack of identifiable aquatic

380   macrofossils and supported by δ^{13}C values.

381   The Unit 2 ages are trustworthy as minimum-limiting constraints on moraine abandonment, but we find the

382   evidence for slumps and rip-up clasts in Unit 2, plus the stratigraphic discordance in radiocarbon ages, reason to

383   doubt the reliability of the radiocarbon ages to reflect the age of the sediment they are within. Our oldest minimum-

384   limiting constraint from Unit 2 is from the macrofossil-rich rip-up clast in 20VIN1 on the Kent Moraine, which

385   holds evidence for two important interpretations: 1) the landscape was ice-free and at least sparsely vegetated as

386   early as 19,350-19,600 cal BP, consistent with our OSL ages suggesting ice sheet retreat by $19.8 \pm 2.6 - 20.6 \pm 2.9$

387   ka, and 2) the landscape stored this long-dead vegetation for thousands of years before it was re-deposited. This age

388   also bolsters our confidence that the MAM is working well in our study area.

389   We use the lowest ages in Unit 3 as minimum limits on the timing of kettle formation and moraine

390   stabilization. The lowest ages from Unit 3 from the Kent Moraine range from 13,650 - 14,050 (20VIN1) to 14,350 -

391 15,050 (21SONG1) cal BP. The lowest ages from Unit 3 from the Lake Escarpment Moraine are 13,600 - 14,000

392 (21LPB1) to 15,000 - 15,400 (13DFK1) cal BP. The range of ages shows the kettles formed through the interval of

393 13,600 to 15,400 cal BP, reflecting the time the moraines stabilized. This shows both moraines stabilized at the same

394 time, even though they are likely several thousand years different in age. Using our OSL ages and minimum-limiting

395 radiocarbon age from Unit 2 to estimate the deposition of the Kent Moraine before 19,350 - 19,600 cal BP, there

396 appears to be a 5 kyr lag time between moraine deposition and stabilization.

397

398 **5.3 A model for kettle basin formation**

399 We propose the following post-glacial history in western New York (Fig. 6). The deposition of the Kent

400 Moraine occurred at least $19.8 \pm 2.6 – 20.6 \pm 2.9$ ka and the landform remained ice-cored for the ensuing 5 – 6 kyr.

401 The deposition of the Lake Escarpment Moraine took place around 17 ka and likewise remained ice-cored for the

402 next 2 – 3 kyr. The hummocky nature of the moraines indicate that they were ice-cored, and we suggest that

403 persistent buried glacial ice prohibited stabilization until well after deposition. Our interpretation is that after ~15 ka

404 buried ice began to melt, and morainal topography – including kettle basins – began to evolve more rapidly (Fig. 6

405 & 7). During the earliest stages of kettle basin formation, there was increased mobilization of sediments from within

406 the uneven ice-rich topography. These initial sediments contained both re-worked and contemporary organic matter

407 from the catchment and were deposited in our study sites as Unit 2. According to this interpretation, our radiocarbon

408 ages from Unit 2 could reflect plant death anytime between moraine deposition and kettle basin stabilization. The

409 13,750 - 15,250 cal BP wood age from basal lake sediments in Nichols Brook is likely another example of delayed

410 kettle formation in this area (Fritz et al., 1987).

411 Moraines can remain ice-cored for thousands of years after deposition due to sediment cover that insulates

412 and preserves the buried ice (Florin and Wright, 1969). If the region is cold enough to support permafrost it may

413 extend the duration that the moraine remains ice-cored (Clayton et al., 2001; Henriksen et al., 2003; Schomacker,

414 2008). Given that the kettles appear to have formed within ~1 kyr of each other, and their formation coincided with

415 the warm Bølling/Allerød period, this suggests the climate during Heinrich Stadial 1 may have been cold enough to

416 help preserve the ice.

417

418
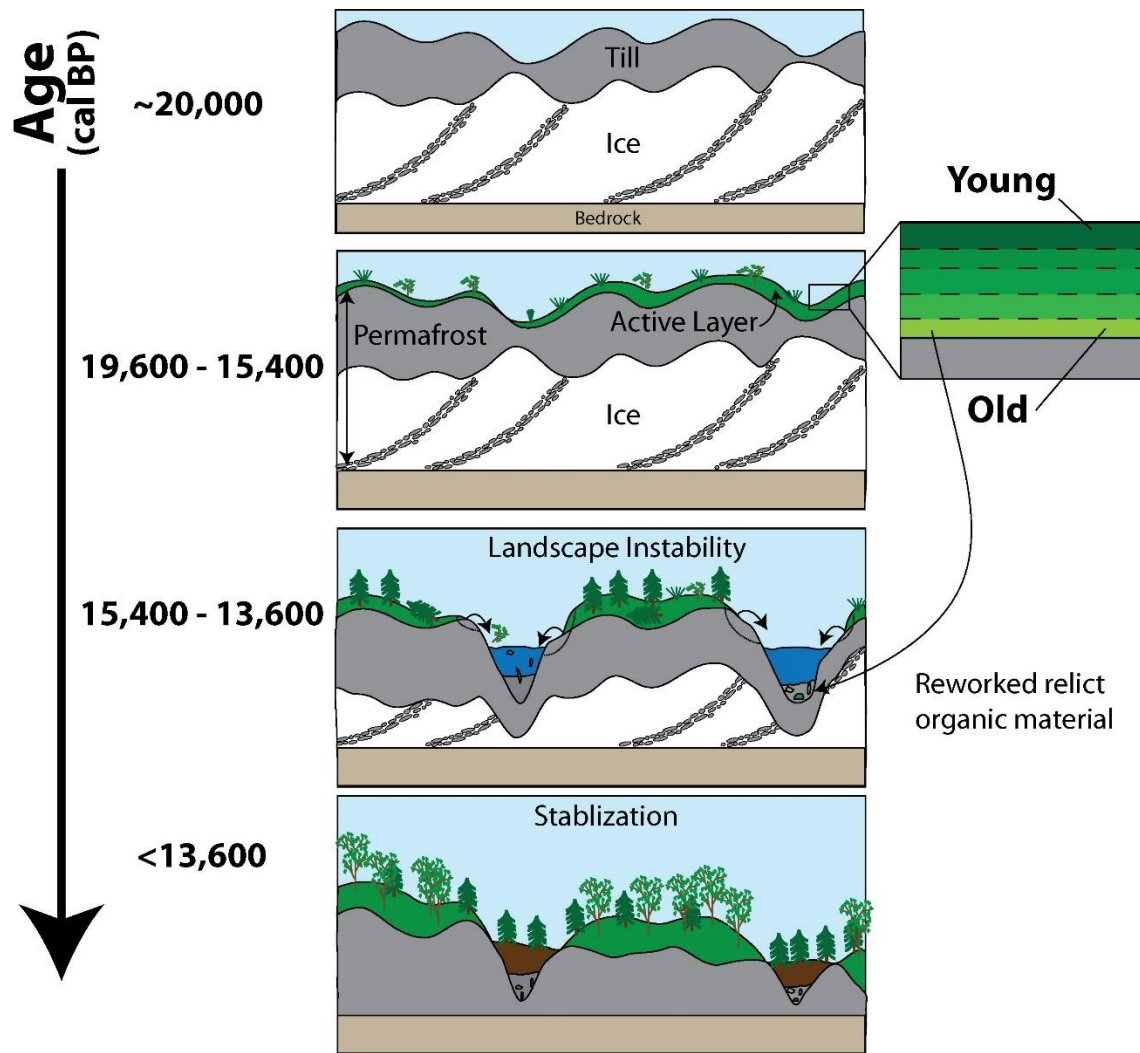
Figure 6. Conceptual model of kettle basin formation of the Kent Moraine in western New York building on Florin and Wright (1969). The same model applies to the Lake Escarpment moraine, except the timeline begins ~17 ka. First, the LIS deposited the ice-cored Kent Moraine. It remained ice-cored, perhaps influenced by permafrost, while tundra vegetation grew atop the moraine and stored carbon in the soil. Next, during climate amelioration in the Bølling-Allerød periods, the ice in the moraine melted. This led to the formation of basins that filled with both contemporaneous and reworked sediments. This is also likely the time when trees and other organic material could be slumped and formed deposits that placed primary tills adjacent to younger material. Finally, organic-rich sediment deposition dominates after ~13.8 ka.

426

5.4 Implications for the climate in western New York

The climate of western New York between 20 and 15 ka is poorly known, but records from Ontario, Ohio, and New England suggest the climate events of the North Atlantic influenced the northeastern U.S. These terrestrial climate reconstructions depict a cold Heinrich Stadial 1 (~18 to ~14.7 ka), a shift to warmer temperatures during the Bølling-Allerød, and a cool Younger Dryas (Gill et al., 2012; Gonzales and Grimm, 2009; Grigg et al., 2021; Shuman et al., 2002; Watson et al., 2018; Yu, 2007; Yu and Eicher, 1998). A stable Heinrich Stadial 1 and shift to warmer temperatures during the Bølling-Allerød is shown by Watson et al. (2018), who used biomarkers (branched-

434   GDGTs) to report that mean annual temperature in central Ohio varied between –2.0 and -0.5 °C from 17.0 to 14.5

435   ka before warming 5°C between 14.5 and 13.0 ka.

436   The rate of LIS retreat offers additional insight into the climate in the northeast US. Barth et al. (2019) used

437   cosmogenic nuclide dating of glacially-transported boulders to estimate LIS thinning in the Adirondack Mountains

438   and showed increased thinning between 15.4 ± 1.0 and 13.9 ± 0.9 ka, generally coincident with the Bølling. The

439   New England Varve Chronology shows a relatively steady net retreat rate of the LIS through the Hudson Valley

440   between 18 and 14.7 ka; during the Bølling the net retreat rate tripled, implying that New England experienced

441   elevated warmth at that time (Ridge et al., 2012).

442   Ice-wedge casts can be used to identify areas that experienced past permafrost and constrain past

443   temperature because their formation requires mean annual temperatures between -6 to -8°C (French, 2007; French

444   and Miller, 2014). Ice-wedge casts are preserved in southern Ontario that were deposited 18-15 ka based on regional

445   correlations (Dalton et al., 2020; Gao, 2005; Morgan et al., 1982). This suggests that the mean annual air

446   temperature was low enough near our study site during Heinrich Stadial 1 to support permafrost. While this

447   temperature depression is larger than reported by Watson et al. (2018), it's likely there was a strong temperature

448   gradient between Ohio and western New York during deglaciation, with the latter remaining within 100 km of the

449   ice margin until 14 ka (Dalton et al., 2020). This proximity to the ice sheet from the LGM to 14 ka may have been a

450   driver of the cold climate that persisted in western New York. There are no reports of relict permafrost features

451   within the LGM limit in western New York, but their presence south of the LGM extent suggest the likelihood of

452   permafrost within the limit as well (French and Millar, 2014).

453   Finally, there are seven local pollen records from Miller (1973), Calkin and McAndrews (1980), and

454   Doody (2018) that describe the initial deglacial vegetation in western New York. Only the Allenberg Bog (Miller,

455   1973) and Dragonfly Kettle (Doody, 2018) pollen records captured a 'tundra' zone at the base, although the

456   presence of both arctic and temperate vegetation complicates their interpretation. The tundra zone is overlain by an

457   interval with high spruce and pine pollen; this is the lowest unit found in the other five records (Miller, 1973; Calkin

458   and McAndrews, 1980). This is likely reflecting the new forest biome associated with warmer temperatures. Given

459   our results, we believe the 'tundra' pollen zone captured both the tundra vegetation that was growing on the moraine

460   prior to basin formation and the more temperate vegetation as spruce and pine moved in during the Bølling.

461   Unfortunately, the pollen records may be unreliable before 14 ka due to the same reworking problems as our

462   radiocarbon dating, but this remains site specific.

463   Altogether, there is evidence that the lag time between ice sheet retreat and kettle basin stabilization may be

464   attributable to sustained permafrost in western New York due to cold North Atlantic conditions during Heinrich

465   Stadial 1 (Fig. 7). The warming at the Bølling onset at ~14.7 ka may have increased regional temperatures, causing

466   the melting of buried ice, initiating a phase of rapid landscape evolution and the formation of kettle basins, and

467   eventually stabilizing the morainal topography. Numerous studies discuss the role of permafrost in the lag time

468   between moraine ages and basal macrofossils along the south-central LIS margin, including Indiana and Illinois

469   (Curry et al., 2018; Fisher et al., 2020), Michigan (Yansa et al., 2020), and Wisconsin (Clayton et al., 2008).

470   Our findings support the observations and conclusions from numerous studies that radiocarbon dates can be
471 extreme minimum age constraints on deglaciation (Curry et al., 2018; Fisher et al., 2020; Florin and Wright, 1969;
472 Halsted et al., 2023; Yansa et al., 2020). In New England, minimum-limiting radiocarbon ages may be the reason for
473 the discrepancy between the timing of moraine deposition as recorded by [10]Be exposure dating (e.g., Balco et al.,
474 2002; Corbett et al., 2017) and radiocarbon ages of basal macrofossils in lakes and bogs (e.g., Peteet et al., 2012).
475 The younger than expected radiocarbon ages from the Valley Heads Moraine from Kozlowski et al. (2018) may be
476 afflicted by similar processes. Permafrost during Heinrich Stadial 1 may have minimized landscape evolution in
477 New England and central New York as well and could help explain the offset.

478
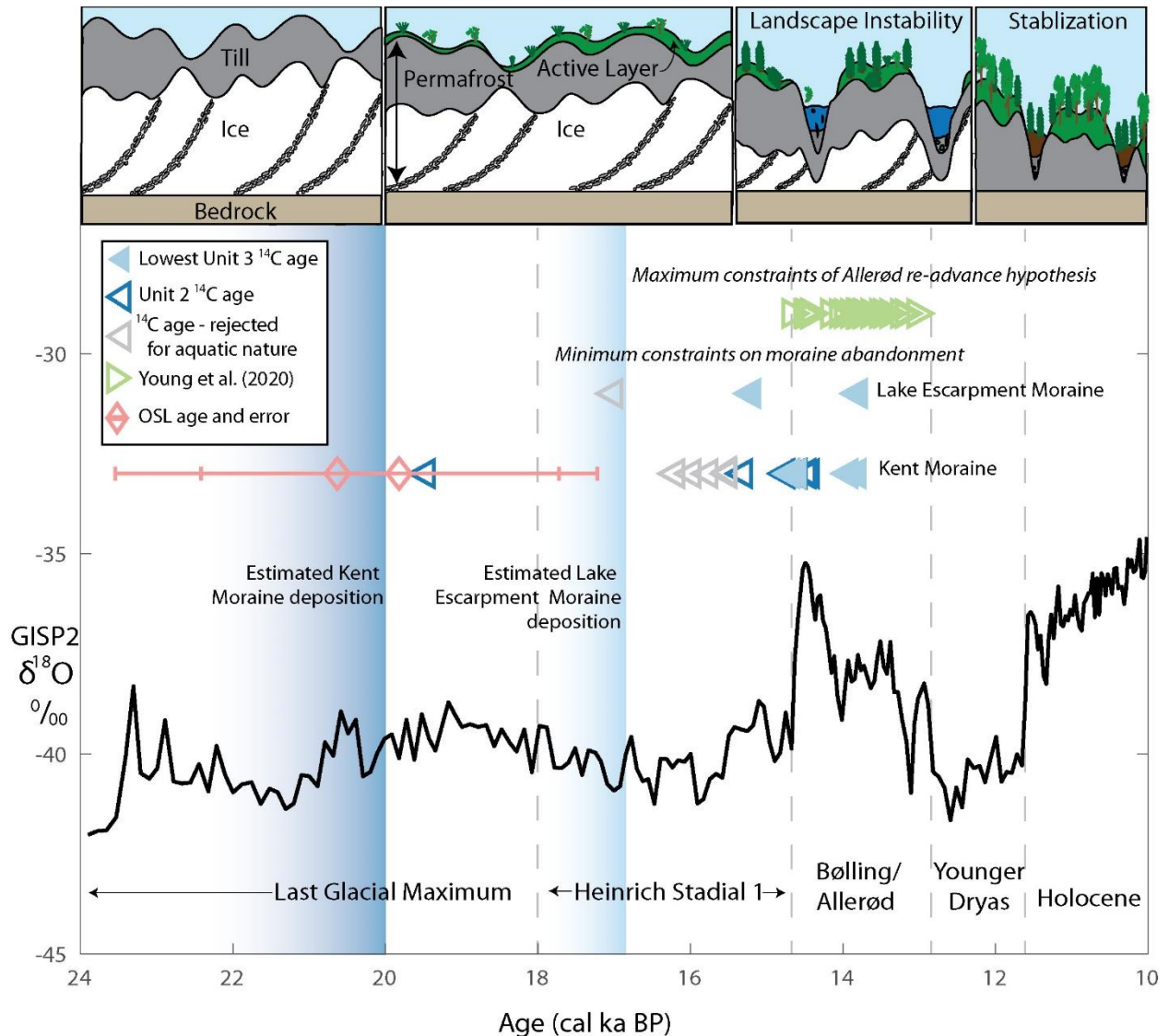
Figure 7. Comparison of radiocarbon ages from the Kent and Lake Escarpment moraine and Young et al. (2020) in the
context of North Atlantic deglacial climate changes. Black line is the GISP2 δ^{18}O record (Grootes and Stuiver, 1999). Dark
blue and light blue fading is the estimated deposition of the Kent Moraine and Lake Escarpment Moraine, respectively.
Dark blue and light blue triangles are Unit 2 and the lowest Unit 3 radiocarbon ages from the Kent and Lake Escarpment
Moraine sediment cores, respectively. Gray triangles are radiocarbon ages that we suspect have hardwater contamination.
Pink diamonds are OSL ages and 2σ errors from the kame delta outboard the Kent Moraine. Green triangles are ages from

485 **Young et al. (2020) interpreted by them to be maximum-limiting constraints on the 13 ka re-advance. Errors for all**
486 **radiocarbon dates are not plotted because their width is smaller than the symbols.**

487

488 **5.5 Allerød re-advance hypothesis**

489   The stratigraphically lowest radiocarbon ages from Unit 3 in the Lake Escarpment Moraine kettle basins,
490 which are 15,000-15,400 and 13,600-14,000 cal BP, pre-date the ~13.1 ka re-advance suggested by Young et al.
491 (2020) (Fig. 5 & 7). Chronologically constrained organic-rich sedimentation, with no stratigraphic evidence of
492 interruption, ensued from at least 13,600-14,000 cal BP and well into the Holocene. Furthermore, there is no
493 evidence of over-compaction in our bulk density measurements in 21LPB1 during this interval of time (Fig. 5).
494 Thus, we do not find evidence that a ~13.1 ka LIS advance created or overran the Lake Escarpment Moraine as
495 hypothesized by Young et al. (2020). Rather, we suggest that the landscape was unstable during its transition from a
496 permafrost-dominated landscape to one with evolving and then stabilizing morainal topography. This landscape
497 instability with reworking of glacial sediments may have led to the stratigraphy interpreted by Young et al. (2020) as
498 primary tills in contact with logs dating to 13 ka (Fig. 7). Both the Dragonfly and Little Protection sites have
499 intervals with increased wood deposition between 14 and 13 ka and future work could investigate the source of these
500 woody intervals to further investigate the results from Young et al. (2020).

501

502 **6 Conclusion**

503   We present 41 new macrofossil-based radiocarbon ages from kettle basin infills in western New York. We
504 find that the lowest radiocarbon ages from Unit 3 (15,000-15,400 and 13,600-14,000 cal BP) are 5 kyr younger than
505 our OSL age constraints on moraine deposition of $19.8 \pm 2.6 – 20.6 \pm 2.9$ ka and the oldest radiocarbon age from
506 Unit 2 of 19,350-19,600 cal BP from the Kent Moraine. The lowest Unit 3 ages are 2 kyr younger than our estimated
507 age of Lake Escarpment Moraine deposition from moraine correlations. We interpret this offset to be due to a cold
508 climate in western New York during Heinrich Stadial 1 supporting persistent buried ice which inhibited kettle basin
509 formation until regional warming that took place during the Bølling. Our results do not support a re-advance of the
510 LIS over the Lake Escarpment Moraine ~13 ka (c.f. Young et al., 2020). The lag time between ice sheet retreat and
511 moraine stabilization in western New York may present an alternate explanation for inconsistencies between basal
512 ages in sediment cores and other dating methods in central New York (Kozlowski et al., 2018) and eastern New
513 York (Peteet et al., 2012).
514   Future work could target features that are stable during ice retreat even where permafrost is present, such as
515 outcrops of pro-glacial and ice-walled lake plane deposits (e.g., Curry et al., 2018), or perhaps moraines that are not
516 hummocky in nature. This limitation may not be as necessary in environments where climate more quickly
517 ameliorated, such as appears to have been the case in southern Ohio (Glover et al., 2011). Additionally, it may be
518 important to consider the coring equipment. The GeoProbe coring device enabled us to collect stiff mineral-rich
519 sediments lower than otherwise possible with the Livingstone and Russian Peat coring devices. This meant that our

520   coring did not stop at first contact with stiff minerogenic sediment that could mistakenly be interpreted as primary

521   glacial in origin.

522

523

524   **Data availability:** Table 2 provides the data to calculate the radiocarbon ages from this study. Table 3 and Table A1

525   provide the data to calculate OSL ages from this study.

526

527   **Author contributions:** JPB and KKP conceptualized the study. ALK and KKP provided funding for fieldwork and

528   lab analyses. KKP, JPB, CKW, BMC, and EPY collected sediment cores. KKP, BMC, EPY and JPB conducted

529   downcore analyses and radiocarbon sampling. CKW collected OSL samples and TMR conducted lab analyses and

530   calculated the ages. KKP compiled and recalculated the radiocarbon ages. KKP, JPB, ALK, CKW, and BMC

531   interpreted the results. KKP wrote the first draft of the manuscript and all authors contributed to editing. KKP and

532   TMR developed the figures and tables.

533

534   **Competing interests.** The authors declare that they have no conflict of interest.

535

536   **Acknowledgements:** We thank the Vincent, Songster, Gebhard, and Bohall families for the access to their property,

537   as well as their enthusiasm and friendship. We thank Joseph Tulenko, Brandon Graham, Elizabeth Thomas, Kurt

538   Lindberg, Owen Cowling, Fiona Ellsworth, Joshua Charlton, Liza Wilson, Jason Parsons, Will Phillips, and George

539   Thomas for their help in the field (it takes a village!). We thank the National Ocean Sciences Accelerator Mass

540   Spectrometry and W. M. Keck Carbon Cycle Accelerator Mass Spectrometer laboratories for radiocarbon analyses.

541   We thank the Luminescence Lab at Utah State University for OSL analyses.

542

543   **Funding sources:** This research was supported by the United State Geological Survey Great Lakes Geological

544   Mapping Coalition grant #G20AC00418, the NSF/GSA Graduate Student Geoscience grant # 13056-21, which was

545   funded by NSF Award # 1949901, and the Mark Diamond Research Fund of the Graduate Student Association of

546   the State University of New York at Buffalo.

547

548   **References**

549   Balco, G., Stone, J. O. H., Porter, S. C., and Caffee, M. W.: Cosmogenic-nuclide ages for New England coastal

550   moraines, Martha's Vineyard and Cape Cod, Massachusetts, USA, Quaternary Science Reviews, 21, 2127–2135,

551   https://doi.org/10.1016/S0277-3791(02)00085-9, 2002.

552   Balco, G., Briner, J., Finkel, R. C., Rayburn, J. A., Ridge, C., and Schaefer, J. M.: Regional beryllium-10 production

553   rate calibration for late-glacial northeastern North America, Quaternary Geochronology, 4, 93-107,

554   https://doi.org/10.1016/j.quageo.2008.09.001, 2009.

555   Barth, A. M., Marcott, S. A., Licciardi, J. M., and Shakun, J. D.: Deglacial Thinning of the Laurentide Ice Sheet in

556   the Adirondack Mountains, New York, USA, Revealed by 36Cl Exposure Dating, Paleoceanography and

557   Paleoclimatology, 34, 946-953, https://doi.org/10.1029/2018PA003477, 2019.

558   Bird, B. and Kozlowski, A.: Late Quaternary Reconstruction of Lake Iroquois in the Ontario Basin of New York.

559   New York State Museum Map & Chart 80, https://www.nysm.nysed.gov/sites/default/files/mc80_iroquois.pdf,

560   2016.

561   Briner, J. P., Cuzzone, J. K., Badgeley, J. A., Young, N. E., Steig, E. J., Morlighem, M., Schlegel, N. J., Hakim, G.

562   J., Schaefer, J. M., Johnson, J. V., Lesnek, A. J., Thomas, E. K., Allan, E., Bennike, O., Cluett, A. A., Csatho, B., de

563   Vernal, A., Downs, J., Larour, E., and Nowicki, S.: Rate of mass loss from the Greenland Ice Sheet will exceed

564   Holocene values this century, Nature, 586, 70-74, https://doi.org/10.1038/s41586-020-2742-6, 2020.

565   Broecker, W. S., Kennett, J. P., Flower, B. P., Teller, J. T., Trumbore, S., Bonani, G., and Wolfli, W.: Routing of

566   meltwater from the Laurentide Ice Sheet during the Younger Dryas cold episode, Nature, 341, 318-321,

567   https://doi.org/10.1038/341318a0, 1989.

568   Calkin, P. E. and Feenstra, B. H.: Evolution of the Erie-Basin Great Lakes, in: Quaternary Evolution of the Great

569   Lakes, edited by: Karrow, P. F., and Calkin, P. E., Geological Society of Canada, https://doi.org/10.1016/0033-

570   5894(87)90011-1, 1985.

571   Calkin, P. E. and McAndrews, J. H.: Geology and paleontology of two late Wisconsin sites in western New York

572   State, Geological Society of America Bulletin, 91, 295-306, https://doi.org/10.1130/0016-

573   7606(1980)91<295:GAPOTL>2.0.CO;2, 1980.

574   Campbell, M. C., Fisher, T. G., and Goble, R. J.: Terrestrial sensitivity to abrupt cooling recorded by aeolian activity

575   in northwest Ohio, USA, Quaternary Research, 75, 411-416, https://doi.org/10.1016/j.yqres.2011.01.009, 2011.

576   Clayton, L. E., Attig, J. W., and Mickelson, D. M.: Effects of late Pleistocene permafrost on the landscape of

577   Wisconsin, USA, Boreas, 30, 173-188, https://doi.org/10.1111/j.1502-3885.2001.tb01221.x, 2001.

578   Corbett, L. B., Bierman, P. R., Stone, B. D., Caffee, M. W., and Larsen, P. L.: Cosmogenic nuclide age estimate for

579   Laurentide Ice Sheet recession from the terminal moraine, New Jersey, USA, and constraints on latest Pleistocene

580   ice sheet history, Quaternary Research, 87, 482-498, https://doi.org/10.1017/qua.2017.11, 2017.

581   Coulombe, S., Fortier, D., Lacelle, D., Kanevskiy, M., and Shur, Y.: Origin, burial and preservation of late

582   Pleistocene-age glacier ice in Arctic permafrost (Bylot Island, NU, Canada), The Cryosphere, 13, 97-111,

583   https://doi.org/10.5194/tc-13-97-2019, 2019.

584 Cronin, T. M., Rayburn, J. A., Guilbault, J. P., Thunell, R., and Franzi, D. A.: Stable isotope evidence for glacial

585 lake drainage through the St. Lawrence Estuary, eastern Canada, ~13.1-12.9 ka, Quaternary International, 260, 55-

586 65, https://doi.org/10.1016/j.quaint.2011.08.041, 2012.

587 Curry, B. B., Lowell, T. V., Wang, H., and Anderson, A. C.: Revised time-distance diagram for the Lake Michigan

588 Lobe, Michigan Subepisode, Wisconsin Episode, Illinois, USA, https://doi.org/10.1130/2018.2530(04), 2018.

589 Dalton, A. S., Margold, M., Stokes, C., Tarasov, L., Dyke, A., Adams, R., Allard, S., Arends, H., Atkinson, N.,

590 Attig, J., Barnett, P., Barnett, R., Batterson, M., Bernatchez, P., Borns, H., Breckenridge, A., Briner, J., Brouard, E.,

591 Campbell, J., and Wright, H.: An updated radiocarbon-based ice margin chronology for the last deglaciation of the

592 North American Ice Sheet Complex, Quaternary Science Reviews, 234, 106223,

593 https://doi.org/10.1016/j.quascirev.2020.106223, 2020.

594 Deevey, E. S., Gross, M. S., Hutchinson, G. E., and Kraybill, H. L.: The Natural 14C Contents of Materials from

595 Hard-Water Lakes, Proceedings of the National Academy of Sciences, 40, 285-288,

596 https://doi.org/10.1073/pnas.40.5.285, 1954.

597 Deuser, W. G. and Degens, E. T.: Carbon Isotope Fractionation in the System

598 CO2(gas)—CO2(aqueous)—HCO3-(aqueous), Nature, 215, 1033-1035,

599 https://doi.org/10.1038/2151033a0, 1967.

600 Donnelly, J. P., Driscoll, N. W., Uchupi, E., Keigwin, L. D., Schwab, W. C., Thieler, E. R., and Swift, S. A.:

601 Catastrophic meltwater discharge down the Hudson Valley: A potential trigger for the Intra-Allerød cold period,

602 Geology, 33, https://doi.org/10.1130/G21043.1, 2005.

603 Doody, E.: A latest pleistocene palynologic record from western New York, Geology, University at Buffalo, 2018.

604 Dyke, A. S.: An outline of North American deglaciation with emphasis on central and northern Canada, in:

605 Developments in Quaternary Sciences, edited by: Ehlers, J., and Gibbard, P. L., Elsevier, 373-424,

606 https://doi.org/10.1016/S1571-0866(04)80209-4, 2004.

607 Elder, K. L., Roberts, M. L., Walther, T., and Xu, L.: Single step Production of graphite from organic Samples for

608 Radiocarbon Measurements, Radiocarbon, 61, 1843-1854, https://doi.org/10.1017/RDC.2019.136, 2019.

609 Eschman, D. F. and Karrow, P. F.: Huron Basin Glacial Lakes: A Review, in: Quaternary Evolution of the Great

610 Lakes, edited by: Karrow, P. F., and Calkin, P. E., Geological Society of Canada, https://doi.org/10.1016/0033-

611 5894(87)90011-1, 1985.

612 Fairchild, H. L. R.: Glacial Waters in Central New York, University of the State of New York1909.

613   Fisher, T. G., Blockland, J. D., Anderson, A., Krantz, D. E., Stierman, D. J., and Goble, R.: Evidence of Sequence

614   and Age of Ancestral Lake Erie Lake-Levels, Northwest Ohio, The Ohio Journal of Science 115,

615   https://doi.org/10.18061/ojs.v115i2.4614, 2015.

616   Fisher, T. G., Dziekan, M. R., McDonald, J., Lepper, K., Loope, H., McCarthy, F. M. G., and Curry, B. B.:

617   Minimum limiting deglacial ages for the out-of-phase Saginaw Lobe of the Laurentide Ice Sheet using optically

618   stimulated luminescence (OSL) and radiocarbon methods, Quaternary Research, 97, 71-87,

619   https://doi.org/10.1017/qua.2020.12, 2020.

620   Florin, M.-B. and Wright, H. E., Jr.: Diatom Evidence for the Persistence of Stagnant Glacial Ice in Minnesota, GSA

621   Bulletin, 80, 695-704, https://doi.org/10.1130/0016-7606(1969)80[695:DEFTPO]2.0.CO;2, 1969.

622   French, H. M.: Surface Features of Permafrost, in: The Periglacial Environment, 116-152,

623   https://doi.org/10.1002/9781118684931.ch6, 2007.

624   French, H. M. and Millar, S. W. S.: Permafrost at the time of the Last Glacial Maximum (LGM) in North America,

625   Boreas, 43, 667-677, https://doi.org/10.1111/bor.12036, 2014.

626   Fritz, P., Morgan, A. V., Eicher, U., and McAndrews, J. H.: Stable isotope, fossil coleoptera and pollen stratigraphy

627   in late quaternary sediments from Ontario and New York state, Palaeogeography, Palaeoclimatology,

628   Palaeoecology, 58, 183-202, https://doi.org/10.1016/0031-0182(87)90059-9, 1987.

629   Fullerton, D. S.: Preliminary correlation of post-Erie interstadial events :(16,000-10,000 radiocarbon years before

630   present), central and eastern Great Lakes region, and Hudson, Champlain, and St. Lawrence Lowlands, United

631   States and Canada, https://doi.org/10.3133/pp1089, 1980.

632   Galbraith, R. F. and Roberts, R. G.: Statistical aspects of equivalent dose and error calculation and display in OSL

633   dating: An overview and some recommendations, Quaternary Geochronology, 11, 1-27,

634   https://doi.org/10.1016/j.quageo.2012.04.020, 2012.

635   Gao, C.: Ice-wedge casts in Late Wisconsinan glaciofluvial deposits, southern Ontario, Canada, Canadian Journal of

636   Earth Sciences, 42, 2117-2126, https://doi.org/10.1139/e05-072, 2005.

637   Gao, C.: Relict Thermal-contraction-crack Polygons and Past Permafrost South of the Late Wisconsinan Glacial

638   Limit in the Mid-Atlantic Coastal Plain, USA, Permafrost and Periglacial Processes, 25, 144-149,

639   https://doi.org/10.1002/ppp.1803, 2014.

640   Gill, J. L., Williams, J. W., Jackson, S. T., Donnelly, J. P., and Schellinger, G. C.: Climatic and megaherbivory

641   controls on late-glacial vegetation dynamics: a new, high-resolution, multi-proxy record from Silver Lake, Ohio,

642   Quaternary Science Reviews, 34, 66-80, https://doi.org/10.1016/j.quascirev.2011.12.008, 2012.

643 Glover, K. C., Lowell, T. V., Wiles, G. C., Pair, D., Applegate, P., and Hajdas, I.: Deglaciation, basin formation and
644 post-glacial climate change from a regional network of sediment core sites in Ohio and eastern Indiana, Quaternary
645 Research, 76, 401-410, https://doi.org/10.1016/j.yqres.2011.06.004, 2011.

646 Gonzales, L. M. and Grimm, E. C.: Synchronization of late-glacial vegetation changes at Crystal Lake, Illinois, USA
647 with the North Atlantic Event Stratigraphy, Quaternary Research, 72, 234-245,
648 https://doi.org/10.1016/j.yqres.2009.05.001, 2009.

649 Grigg, L. D., Engle, K. J., Smith, A. J., Shuman, B. N., and Mandl, M. B.: A multi-proxy reconstruction of climate
650 during the late-Pleistocene to early Holocene transition in the northeastern, USA, Quaternary Research, 102, 188-
651 204, https://doi.org/10.1017/qua.2020.127, 2021.

652 Grootes, P. M. and Stuiver, M.: GISP2 Oxygen Isotope Data, PANGAEA [dataset],
653 https://doi.org/10.1594/PANGAEA.56094, 1999.

654 Halsted, C. T., Bierman, P. R., Shakun, J. D., Davis, P. T., Corbett, L. B., Drebber, J. S., and Ridge, J. C.: A critical
655 re-analysis of constraints on the timing and rate of Laurentide Ice Sheet recession in the northeastern United States,
656 Journal of Quaternary Science, https://doi.org/10.1002/jqs.3563, 2023.

657 Heath, S. L., Loope, H. M., Curry, B. B., and Lowell, T. V.: Pattern of southern Laurentide Ice Sheet margin
658 position changes during Heinrich Stadials 2 and 1, Quaternary Science Reviews, 201, 362-379,
659 https://doi.org/10.1016/j.quascirev.2018.10.019, 2018.

660 Heiri, O., Lotter, A. F., and Lemcke, G.: Loss on ignition as a method for estimating organic and carbonate content
661 in sediments: reproducibility and comparability of results, Journal of Paleolimnology, 25, 101-110,
662 https://doi.org/10.1023/A:1008119611481, 2001.

663 Henriksen, M., Mangerud, J., Matiouchkov, A., Paus, A., and Svendsen, J. I.: Lake stratigraphy implies an 80 000 yr
664 delayed melting of buried dead ice in northern Russia, Journal of Quaternary Science, 18, 663-679,
665 https://doi.org/10.1002/jqs.788, 2003.

666 Higley, M. C., Fisher, T. G., Jol, H. M., Lepper, K., and Martin-Hayden, J. M.: Stratigraphic and chronologic
667 analysis of the Warren Beach, northwest Ohio, USA, Canadian Journal of Earth Sciences, 51, 737-749,
668 https://doi.org/10.1139/cjes-2014-0047, 2014.

669 Keeley, J. E. and Sandquist, D. R.: Carbon: freshwater plants, Plant Cell & Environment, 15,
670 https://doi.org/10.1111/j.1365-3040.1992.tb01653.x, 1992.

671 Kozlowski, A. L., Bird, B. C., Lowell, T. V., Smith, C. A., Feranec, R. S., and Graham, B. L.: Minimum age of the
672 Mapleton, Tully, and Labrador Hollow moraines indicates correlation with the Port Huron Phase in central New

673 York State, in: Quaternary Glaciation of the Great Lakes Region: Process, Landforms, Sediments, and Chronology,

674 https://doi.org/10.1130/2018.2530(10), 2018.

675 LaFleur, R. G.: Glacial geology and stratigraphy of Western New York Nuclear Service Center and vicinity,

676 Cattaraugus and Erie Counties, New York, Report 79-989, https://doi.org/10.3133/ofr79989, 1979.

677 Last, W. and Smol, J.: Tracking environmental change using lake sediments. 2. Physical and geochemical methods,

678 https://doi.org/10.1007/0-306-47670-3, 2001.

679 Lewis, C. F. M. and Anderson, T. W.: A younger glacial Lake Iroquois in the Lake Ontario basin, Ontario and New

680 York: re-examination of pollen stratigraphy and radiocarbon dating, Canadian Journal of Earth Sciences, 57, 453-

681 463, https://doi.org/10.1139/cjes-2019-0076, 2019.

682 Leydet, D. J., Carlson, A. E., Teller, J. T., Breckenridge, A., Barth, A. M., Ullman, D. J., Sinclair, G., Milne, G. A.,

683 Cuzzone, J. K., and Caffee, M. W.: Opening of glacial Lake Agassiz's eastern outlets by the start of the Younger

684 Dryas cold period, Geology, 46, 155-158, https://doi.org/10.1130/G39501.1, 2018.

685 Löfverström, M., Caballero, R., Nilsson, J., and Kleman, J.: Evolution of the large-scale atmospheric circulation in

686 response to changing ice sheets over the last glacial cycle, Climate of the Past, 10, 1453-1471,

687 https://doi.org/10.5194/cp-10-1453-2014, 2014.

688 Lusch, D. P., Stanley, K. E., Schaetzl, R. J., Kendall, A. D., Van Dam, R. L., Nielsen, A., Blumer, B. E., Hobbs, T.

689 C., Archer, J. K., Holmstadt, J. L. F., and May, C. L.: Characterization and Mapping of Patterned Ground in the

690 Saginaw Lowlands, Michigan: Possible Evidence for Late-Wisconsin Permafrost, Annals of the Association of

691 American Geographers, 99, 445-466, https://doi.org/10.1080/00045600902931629, 2009.

692 MacClintock, P. and Apfel, E. T.: Correlation of the drifts of the Salamanca re-entrant, New York, Bulletin of the

693 Geological Society of America, 55, 1143-1164, https://doi.org/10.1130/GSAB-55-1143, 1944.

694 Miller, N. G.: Late-glacial and postglacial vegetation change in southwestern New York State, University of the

695 State of New York, State Education Dept, Albany, https://www.biodiversitylibrary.org/bibliography/135533, 1973.

696 Morgan, A. V.: Distribution and probable age of relict permafrost features in south-western Ontario, 4th Canadian

697 Permafrost Conference, Ottawa, Ontario, 91-100,

698 Muller, E. H. and Calkin, P. E.: Timing of Pleistocene glacial events in New York State, Canadian Journal of Earth

699 Sciences, 30, 1829-1845, https://doi.org/10.1139/e93-161, 1993.

700 Muller, E. H. and Prest, V. K.: Glacial Lakes in the Ontario Basin, in: Quaternary Evolution of the Great Lakes

701 edited by: Karrow, P. F., and Calkin, P., E.,, Geological Society of Canada, https://doi.org/10.1016/0033-

702 5894(87)90011-1, 1985.

703   Murray, A. S. and Wintle, A. G.: Luminescence dating of quartz using an improved single-aliquot regenerative-dose

704   protocol, Radiation Measurements, 32, 57-73, https://doi.org/10.1016/S1350-4487(99)00253-X, 2000.

705   Oana, S. and Deevey, E. S.: Carbon 13 in lake waters and its possible bearing on paleolimnology, American Journal

706   of Science, 258-A, 253-272, 1960.

707   Olley, J. M., Caitcheon, G. G., and Roberts, R. G.: The origin of dose distributions in fluvial sediments, and the

708   prospect of dating single grains from fluvial deposits using optically stimulated luminescence, Radiation

709   Measurements, 30, 207-217, https://doi.org/10.1016/S1350-4487(99)00040-2, 1999.

710   Olsson, I.: Radiometric Methods, in: Handbook of Holocene paleoecology and paleohydrology, edited by: Berglund,

711   B., John Wiley & Sons, Chichester, 273-312, https://doi.org/10.1002/gea.3340040208, 1986.

712   Osman, M. B., Tierney, J. E., Zhu, J., Tardif, R., Hakim, G. J., King, J., and Poulsen, C. J.: Globally resolved

713   surface temperatures since the Last Glacial Maximum, Nature, 599, 239-244, https://doi.org/10.1038/s41586-021-

714   03984-4, 2021.

715   Pearson, A., McNichol, A. P., Schneider, R. J., Von Reden, K. F., and Zheng, Y.: Microscale AMS 14C

716   Measurement at NOSAMS, Radiocarbon, 40, 61-75, https://doi.org/10.1017/S0033822200017902, 1997.

717   Peteet, D. M., Beh, M., Orr, C., Kurdyla, D., Nichols, J., and Guilderson, T.: Delayed deglaciation or extreme Arctic

718   conditions 21-16 cal. kyr at southeastern Laurentide Ice Sheet margin?, Geophysical Research Letters, 39, n/a-n/a,

719   https://doi.org/10.1029/2012GL051884, 2012.

720   Porreca, C., Briner, J. P., and Kozlowski, A.: Laurentide ice sheet meltwater routing along the Iro-Mohawk River,

721   eastern New York, USA, Geomorphology, 303, 155-161, https://doi.org/10.1016/j.geomorph.2017.12.001, 2018.

722   Ramsey, K.: Geologic map of New Castle county, Delaware: Delaware Geological Survey Geologic Map Series, 13,

723   2005.

724   Ramsey, K.: Geologic map of Kent County, Delaware: Delaware Geological Survey Geologic Map Series, 2007.

725   Rayburn, J. A., Franzi, D. A., and Knuepfer, P. L. K.: Evidence from the Lake Champlain Valley for a later onset of

726   the Champlain Sea and implications for late glacial meltwater routing to the North Atlantic, Palaeogeography,

727   Palaeoclimatology, Palaeoecology, 246, 62-74, https://doi.org/10.1016/j.palaeo.2006.10.027, 2007.

728   Rayburn, J. A., K. Knuepfer, P. L., and Franzi, D. A.: A series of large, Late Wisconsinan meltwater floods through

729   the Champlain and Hudson Valleys, New York State, USA, Quaternary Science Reviews, 24, 2410-2419,

730   https://doi.org/10.1016/j.quascirev.2005.02.010, 2005.

Rayburn, J. A., Cronin, T. M., Franzi, D. A., Knuepfer, P. L. K., and Willard, D. A.: Timing and duration of North American glacial lake discharges and the Younger Dryas climate reversal, Quaternary Research, 75, 541-551, https://doi.org/10.1016/j.yqres.2011.02.004, 2011.

Reimer, P. J., Austin, W. E. N., Bard, E., Bayliss, A., Blackwell, P. G., Bronk Ramsey, C., Butzin, M., Cheng, H., Edwards, R. L., Friedrich, M., Grootes, P. M., Guilderson, T. P., Hajdas, I., Heaton, T. J., Hogg, A. G., Hughen, K. A., Kromer, B., Manning, S. W., Muscheler, R., Palmer, J. G., Pearson, C., van der Plicht, J., Reimer, R. W., Richards, D. A., Scott, E. M., Southon, J. R., Turney, C. S. M., Wacker, L., Adolphi, F., Büntgen, U., Capano, M., Fahrni, S. M., Fogtmann-Schulz, A., Friedrich, R., Köhler, P., Kudsk, S., Miyake, F., Olsen, J., Reinig, F., Sakamoto, M., Sookdeo, A., and Talamo, S.: The IntCal20 Northern Hemisphere Radiocarbon Age Calibration Curve (0–55 cal kBP), Radiocarbon, 62, 725-757, https://doi.org/10.1017/RDC.2020.41, 2020.

Richard, P. J. H. and Occhietti, S.: 14C chronology for ice retreat and inception of Champlain Sea in the St. Lawrence Lowlands, Canada, Quaternary Research, 63, 353-358, https://doi.org/10.1016/j.yqres.2005.02.003, 2005.

Ridge, J. C.: The last deglaciation of the northeastern United States: a combined varve, paleomagnetic, and calibrated 14C chronology, in: Geoarchaeology of landscapes in the glaciated northeast, edited by: Hart, J. P., and Cremeens, D. L., New York State Museum Bulletin, 15-45, 2003.

Ridge, J. C., Balco, G., Bayless, R. L., Beck, C. C., Carter, L. B., Dean, J. L., Voytek, E. B., and Wei, J. H.: The new North American Varve Chronology: A precise record of southeastern Laurentide Ice Sheet deglaciation and climate, 18.2-12.5 kyr BP, and correlations with Greenland ice core records, American Journal of Science, 312, 685-722, https://doi.org/10.2475/07.2012.01, 2012.

Rittenour, T. M., Cotter, J. F. P., and Arends, H. E.: Application of single-grain OSL dating to ice-proximal deposits, glacial Lake Benson, west-central Minnesota, USA, Quaternary Geochronology, 30, 306-313, https://doi.org/10.1016/j.quageo.2015.02.025, 2015.

Schomacker, A.: What controls dead-ice melting under different climate conditions? A discussion, Earth-Science Reviews, 90, 103-113, https://doi.org/10.1016/j.earscirev.2008.08.003, 2008.

Shah Walter, S. R., Gagnon, A. R., Roberts, M. L., McNichol, A. P., Gaylord, M. C. L., and Klein, E.: Ultra-Small Graphitization Reactors for Ultra-Microscale 14C Analysis at the National Ocean Sciences Accelerator Mass Spectrometry (NOSAMS) Facility, Radiocarbon, 57, 109-122, https://doi.org/10.2458/azu_rc.57.18118, 2015.

Shuman, B., Webb Iii, T., Bartlein, P., and Williams, J. W.: The anatomy of a climatic oscillation: vegetation change in eastern North America during the Younger Dryas chronozone, Quaternary Science Reviews, 21, 1777-1791, https://doi.org/10.1016/S0277-3791(02)00030-6, 2002.

761 Stanford, S. D., Stone, B. D., Ridge, J. C., Witte, R. W., Pardi, R. R., and Reimer, G. E.: Chronology of Laurentide
762 glaciation in New Jersey and the New York City area, United States, Quaternary Research, 1-26,
763 https://doi.org/10.1017/qua.2020.71, 2020.

764 Stuiver, M. and Polach, H. A.: Discussion Reporting of 14C Data, Radiocarbon, 19, 355-363,
765 https://doi.org/10.1017/S0033822200003672, 1977.

766 Stuiver, M. and Reimer, P. J.: Extended 14C Data Base and Revised CALIB 3.0 14C Age Calibration Program,
767 Radiocarbon, 35, 215-230, https://doi.org/10.1017/S0033822200013904, 1993.

768 Teller, J. T.: Controls, history, outbursts, and impact of large late-Quaternary proglacial lakes in North America, in:
769 The Quaternary Period in the United States, Developments in Quaternary Sciences, 45-61,
770 https://doi.org/10.1016/S1571-0866(03)01003-0, 2003.

771 Terasmae, J.: Some problems of late Wisconsin history and geochronology in southeastern Ontario, Canadian
772 Journal of Earth Sciences, 17, 361-381, https://doi.org/10.1139/e80-035, 1980.

773 Tulenko, J. P., Lofverstrom, M., and Briner, J. P.: Ice sheet influence on atmospheric circulation explains the
774 patterns of Pleistocene alpine glacier records in North America, Earth and Planetary Science Letters, 534, 116115,
775 https://doi.org/10.1016/j.epsl.2020.116115, 2020.

776 US Geological Survey: FGDC Digital Cartographic Standard for Geologic Map Symbolization (PostScript
777 Implementation), http://pubs.usgs.gov/tm/2006/11A02/, 2006.

778 Vogel, J. S., Southon, J. R., Nelson, D. E., and Brown, T. A.: Performance of catalytically condensed carbon for use
779 in accelerator mass spectrometry, Nuclear Instruments and Methods in Physics Research Section B: Beam
780 Interactions with Materials and Atoms, 5, 289-293, https://doi.org/10.1016/0168-583X(84)90529-9, 1984.

781 Wang, Y. and Wooller, M. J.: The stable isotopic (C and N) composition of modern plants and lichens from northern
782 Iceland: with ecological and paleoenvironmental implications, Jökull, 56, 27-38, 10.33799/jokull2006.56.027, 2006.

783 Watson, B. I., Williams, J. W., Russell, J. M., Jackson, S. T., Shane, L., and Lowell, T. V.: Temperature variations
784 in the southern Great Lakes during the last deglaciation: Comparison between pollen and GDGT proxies,
785 Quaternary Science Reviews, 182, 78-92, https://doi.org/10.1016/j.quascirev.2017.12.011, 2018.

786 Wright, H. E. and Stefanova, I.: Plant trash in the basal sediments of glacial lakes, Acta Palaeobotanica, 44, 141-
787 146, 2004.

788 Yansa, C. H., II, F. A. E., Schaetzl, R. J., Kettle, J. M., and Arbogast, A. F.: Interpreting basal sediments and plant
789 fossils in kettle lakes: insights from Silver Lake, Michigan, USA, Canadian Journal of Earth Sciences, 57, 292-305,
790 https://doi.org/10.1139/cjes-2018-0338, 2020.

791   Young, R. A., Gordon, L. M., Owen, L. A., Huot, S., and Zerfas, T. D.: Evidence for a late glacial advance near the

792   beginning of the Younger Dryas in western New York State: An event postdating the record for local Laurentide ice

793   sheet recession, Geosphere, https://doi.org/10.1130/GES02257.1, 2020.

794   Yu, Z.: Rapid response of forested vegetation to multiple climatic oscillations during the last deglaciation in the

795   northeastern United States, Quaternary Research, 67, 297-303, https://doi.org/10.1016/j.yqres.2006.08.006, 2007.

796   Yu, Z. and Eicher, U.: Abrupt Climate Oscillations During the Last Deglaciation in Central North America, Science,

797   282, 2235-2238, doi:10.1126/science.282.5397.2235, 1998.